



Supplement of

Measurements of higher alkanes using NO⁺ chemical ionization in PTR-ToF-MS: important contributions of higher alkanes to secondary organic aerosols in China

Chaomin Wang et al.

Correspondence to: Bin Yuan (byuan@jnu.edu.cn) and Min Shao (mshao@pku.edu.cn)

The copyright of individual parts of the supplement might differ from the CC BY 4.0 License.

26 **Page S1-S50**

27 **Contents of this file**

28 Appendix 5

29 Figures S1 to S31

30 Table S1-S4

31 Appendix 1 Description of sampling sites

32 Appendix 2 Estimation of SOA production from individual precursors

33 Appendix 3 Estimation of contributions of individual precursors to SOA production

34 Appendix 4 Calculation of OH exposure

35 Appendix 5 Estimation of SOA production rate from individual precursors

36 Figure S1. Sampling site locations of Guangzhou Campaign in PRD and Baoding Campaign

37 in NCP of China.

38 Figure S2. The variations of NO^+ , H_3O^+ , O_2^+ and NO_2^+ ions on the voltages of ion source (U_s and U_{so}) for NO^+ PTR-ToF-MS. For each experiment, either U_s or U_{so} is fixed at a voltage and the other was varied to explore the best setting for NO^+ PTR-ToF-MS. For example, test #1 in (a), we fix U_s at 40 V and change U_{so} from 20 V to 180 V. The dashed line in (a) indicate the setting point in this study ($U_s=40$ V and $U_{so}=100$ V).

43 Figure S3. Time series of NO^+ , H_3O^+ , O_2^+ , NO_2^+ during the PRD (a) and the NCP (b) campaigns, respectively.

45 Figure S4. Time series of O_2^+ to NO^+ ratio and the absolute humidity during the PRD (a) and the NCP (b) campaigns, respectively.

47 Figure S5. Humidity dependence of O_2^+ to NO^+ ratios during the lab experiment and the two field campaigns.

49 Figure S6. Calibration factors of C8-C15 *n*-alkanes under dry conditions (RH<1%) during the two field campaigns.

51 Figure S7. Humidity dependence of all product ions and the fragment ions for *n*-alkanes (C8-
52 C15) standards (a), and primary ions (NO^+ , O_2^+ , H_3O^+) (b).

53 Figure S8. Mass spectra of the distributions of product ions from *n*-Dodecane (**a**), *n*-
54 Pentadecane (**b**) and *n*-Eicosane (**c**) with NO^+ PTR-ToF-MS. The signals of masses shown
55 here are the results after subtracting the isotopic signals.

56 Figure S9. Fraction of product ions ($m-1$)⁺ in the mass spectra of *n*-alkanes and their isomers
57 with different number of substituted methyl groups in NO^+ PTR-ToF-MS.

58 Figure S10. Delay times of higher alkanes for the field campaigns, emission source
59 measurements and tubing losses test in the laboratory.

60 Figure S11. An example of the voltages of ion source voltages (U_s , U_{so}), drift tube (U_{drift} ,
61 U_{dx}) and pressure of drift tube (a), and the signal changes of primary ions (b) during
62 automatical switching between NO^+ mode and H_3O^+ mode, respectively.

63 Figure S12. The tubing loss experiments of higher alkanes (*n*-C8-C15), 1,2,4-
64 trimethylbenzene, α -pinene and naphthalene at room temperature using PTR-ToF-MS with an
65 external pump at 5.0 L/min.

66 Figure S13. Comparisons of benzene, toluene, C8 aromatics and C9 aromatics measured by
67 NO^+ PTR-ToF-MS (red dots), H_3O^+ PTR-ToF-MS (blue dots) and GC-MS/FID (green lines
68 and dots) during the PRD campaign.

69 Figure S14. Comparisons of acetaldehyde, pentanone, ethanol and acrolein measured by NO^+
70 PTR-ToF-MS (red dots) and H_3O^+ PTR-ToF-MS (blue dots) during the PRD and NCP
71 campaigns.

72 Figure S15. Comparisons of C9-C11 alkanes measured by NO^+ PTR-ToF-MS and GC-
73 MS/FID during PRD campaign.

74 Figure S16. Diurnal variations of OH concentrations in PRD and NCP, respectively. OH
75 concentrations are derived from an observation-constrained box model utilizing MCM v3.3.1
76 as the chemical mechanisms(Wolfe et al., 2016).

77 Figure S17. Similar diurnal profiles of C8-C21 alkanes during campaigns in PRD (a, b) and
78 NCP (c, d).

79 Figure S18. Comparisons of average diurnal variations of OH exposure calculated from the
80 ratio of m+p-xylene and ethylbenzene for anthropogenic compounds in PRD and NCP and
81 isoprene chemistry in PRD for biogenic compounds.

82 Figure S19. (a) Time series of isoprene and monoterpenes in NCP. (b) Diurnal variation of
83 isoprene, monoterpenes and benzene in NCP. (c) Scatter plot of isoprene and monoterpenes
84 versus CO in NCP.

85 Figure S20. Time series of naphthalene, methylnaphthalenes, dimethylnaphthalenes in PRD (a)
86 and NCP (b), respectively.

87 Figure S21. Diurnal variations of concentrations of organic aerosols (OA), secondary organic
88 aerosols (SOA) and primary organic aerosols (POA) in PRD (a) and NCP (b). POA and SOA
89 were determined by positive matrix factorization (PMF) analysis of OA measured by AMS.

90 Figure S22. The reported SOA yields as a function of OA concentrations for higher alkanes
91 (C8-C21 alkanes) (a-k) under high-NO_x condition from chamber studies(Lim and Ziemann,
92 2009;Presto et al., 2010a;Tkacik et al., 2012;Loza et al., 2014;Lamkaddam et al., 2017b).

93 Figure S23. The reported SOA yields as a function of OA concentrations for monoaromatics
94 (benzene, toluene, m-xylene, 1,2,3-TMB/1,2,4-TMB/1,3,5-TMB, styrene)(Ng et al., 2007;Li
95 et al., 2016;Tajuelo et al., 2019) (a-e), naphthalenes (naphthalene, methylnaphthalene,
96 dimethylnaphthalenes) (Chan et al., 2009) (f-h) and isoprenoids (isoprene and α-
97 pinene)(Carlton et al., 2009;Edney et al., 2005;Kleindienst et al., 2006;Pandis et al.,
98 1991;Ahlberg et al., 2017) (i-j) under high-NO_x condition from chamber studies.

99 Figure S24. Time series of NO_x (NO, NO₂) during the PRD (a) and the NCP (b) campaigns,
100 respectively.

101 Figure S25. Time series of SOA produced from higher alkanes (C8-C21 alkanes),
102 monoaromatics (benzene, toluene, C8 aromatics, C9 aromatics and styrene), naphthalenes
103 (naphthalene, methylnaphthalenes, dimethylnaphthalenes) and isoprenoids (isoprene and
104 monoterpenes) as well as the measured SOA concentrations in PRD (a) and NCP (b),
105 respectively.

106 Figure S26. Scatter plots of total SOA production from higher alkanes (C8-C21 alkanes),
107 monoaromatics (benzene, toluene, C8 aromatics, C9 aromatics and styrene), naphthalenes
108 (naphthalene, methylnaphthalenes, dimethylnaphthalenes) and isoprenoids (isoprene and
109 monoterpenes) versus measured SOA concentrations during the PRD campaign (a) and NCP
110 campaign (b).

111 Figure S27. The relative contributions to measured SOA concentrations from higher alkanes
112 (C8-C21 alkanes), monoaromatics (benzene, toluene, C8 aromatics, C9 aromatics and styrene),
113 naphthalenes (naphthalene, methylnaphthalenes, dimethylnaphthalenes) and isoprenoids
114 (isoprene and monoterpenes) in PRD (a) and NCP (b).

115 Figure S28. The average concentrations from higher alkanes (C8-C21 alkanes), monoaromatics
116 (benzene, toluene, C8 aromatics, C9 aromatics and styrene), naphthalenes (naphthalene,
117 methylnaphthalenes, dimethylnaphthalenes) and isoprenoids (isoprene and monoterpenes) in
118 PRD (a) and NCP (b), respectively.

119 Figure S29. Diurnal variations of SOA yields of *n*-C15 alkane, benzene, naphthalene and α -
120 pinene in PRD (a) and NCP (b).

121 Figure S30. The mean SOA production rates of higher alkanes (C8-C20 alkanes),
122 monoaromatics (benzene, toluene, C8 aromatics, C9 aromatics and styrene), naphthalenes
123 (naphthalene, methylnaphthalenes, dimethylnaphthalenes) and isoprenoids (isoprene and

124 monoterpenes) and their hourly diurnal variations in PRD (a) and NCP (b). Diurnal variations
125 of alkanes, monoaromatics, naphthalenes and isoprenoids in PRD (c) and NCP (d).

126 Figure S31. Correlation of m+p-xylene with ethylbenzene in PRD (a) and NCP (b). The dashed
127 lines in both graphs indicate the estimated initial mission ratio of m+p-xylene/ethylbenzene.

128 Table S1. The settings of the voltages of ion source voltages (Us, Uso), drift tube (Udrift, Udx)
129 and pressure of drift tube (pDrift) during automatical switching between NO^+ mode and H_3O^+
130 mode, respectively.

131 Table S2. Fractions of *n*-alkanes in higher alkanes with same formulas derived from this study,
132 ambient air in Los Angeles, Bakersfield, Caldecott Tunnel and in vehicle exhausts.

133 Table S3. The calculated average SOA yields of higher alkanes in PRD and NCP.

134 Table S4. Average biases in SOA yields due to vapor wall losses for various VOCs under high-
135 NO_x conditions from Zhang et al. 2014.

136

137 **1. Description of sampling sites**

138 The sampling site of Guangzhou Campaign (23.13° N, 113.26° E) was on the top of a
139 nine-story building (25 m above ground level) at Guangzhou Institute of Geochemistry,
140 Chinese Academy of Sciences. This site is a typical urban site surrounded by residential
141 areas, campus and urban transport arteries with a strong influence of vehicle
142 emissions. Field measurements of site Baoding (38.85° N, 115.48° E) were performed on
143 the top of a sea container (3.5 m above ground level) located at a Meteorological Auto-
144 Monitoring Station in the rural area of North China Plain. This rural site was surrounded by
145 farmlands and villages, with several national roads and railways nearby, where air masses
146 are influenced from local emissions and regional transport.

147 **2. Estimation of SOA production from individual precursors**

148 It is assumed that VOCs are removed from the atmosphere mainly by reaction with OH
149 radical(Atkinson and Arey, 2003), then the VOCs are assumed to follow a pseudo first-order
150 kinetic reaction, such as

$$151 \quad -\frac{d[VOC_i]}{dt} = k_{VOC_i}[VOC_i][OH] \quad (S1)$$

152 Where $[VOC_i]$ is the concentration of a given VOC ($\mu\text{g m}^{-3}$), $[\text{OH}]$ is the concentration of
153 OH radical (molecule cm^{-3}), k_{VOC_i} is the rate constant of VOC_i with the OH radical (cm^3
154 $\text{molecule}^{-1} \text{s}^{-1}$). The initial concentration of a given VOC, $[VOC_i]_{t=0}$ can be retrieved from
155 Eq. (1) as follows:

$$156 \quad [VOC_i]_{t=0} = [VOC_i]_t \times (e^{k_{VOC_i} \times [\text{OH}] \times \Delta t}) \quad (S2)$$

157 $[VOC_i]_t$ is the VOC_i concentration measured at time t ($\mu\text{g m}^{-3}$), The OH exposure, $[\text{OH}] \times \Delta t$
158 ($\text{molecules cm}^{-3} \text{s}$), is estimated by the ratio of 1,2,4-trimethylbenzene to benzene(de Gouw
159 et al., 2017; Hayes et al., 2013) for anthropogenic VOCs and by isoprene chemistry method

160 for biogenic VOCs, respectively (Apel et al., 2002; Roberts et al., 2006) (see details in SI,
 161 Appendix 4 and Figure S19). Then consumed concentration of a given VOC, $\Delta[VOC_i]$, can
 162 be estimated as follows:

$$163 \quad \Delta[VOC_i] = [VOC_i]_{t=0} - [VOC_i]_t \quad (\text{S3})$$

$$164 \quad \Delta[VOC_i] = [VOC_i]_t \times (e^{k_{voc_i} \times ([OH] \times \Delta t)} - 1) \quad (\text{S4})$$

165 Then for a given VOC, the SOA production ($\mu\text{g m}^{-3}$) at time t , $[SOA_i]_t$, can be estimated
 166 using the consumed concentration multiply the SOA yield, $Yield_i$, as follows:

$$167 \quad [SOA_i]_t = [VOC_i]_t \times (e^{k_{voc_i} \times ([OH] \times \Delta t)} - 1) \times Yield_i \quad (\text{S5})$$

168 3. Estimation of contributions of individual precursors to SOA production

169 We calculated the relative contribution of each compound to the total SOA
 170 concentration at time t by

$$171 \quad [Fraction_i]_t = \frac{[SOA_i]_t}{[SOA_{measured}]_t} \times 100 \quad (\text{S6})$$

172 where $[Fraction_i]_t$ (%) is the relative contribution of a given compound VOC_i to the
 173 measured SOA total concentration, $[SOA_i]_t$ is the SOA production of VOC_i at time t by the
 174 equation (S6), $[SOA_{measured}]_t$ is the SOA concentration at time t , which is determined by
 175 positive matrix factorization (PMF) analysis of organic aerosol measured by aerosol mass
 176 spectrometry ($\mu\text{g m}^{-3}$).

177 4. Calculation of OH exposure

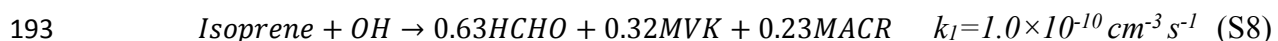
178 The observed ratios between m+p-xylene and ethylbenzene were used to estimate the
 179 OH exposure ($[OH] \times \Delta t$) for anthropogenic compounds by Roberts et al. (1984):

$$180 \quad [OH] \times \Delta t = \frac{1}{k_{m+p-xylene} - k_{ethylbenzene}} \times [\ln(\frac{m+p-xylene}{ethylbenzene})_{t=0} - \ln(\frac{m+p-xylene}{ethylbenzene})_t], \quad (\text{S7})$$

181 where the initial emission ratios of m+p-xylene/ethylbenzene were estimated according to the
182 correlation of m+p-xylene with ethylbenzene during campaigns. The ratio of 4 and 1.5 were
183 used in the PRD campaign and the NCP campaign, respectively (Figure S31).

184 During 2018 PRD campaign, isoprenoids (i.e. isoprene and monoterpenes in this study)
185 are dominantly emitted from biogenic sources, which are different from anthropogenic
186 compounds such as higher alkanes, monoaromatics and naphthalenes. Therefore, we calculated
187 the OH exposure of isoprenoids based on isoprene chemistry for 2018 PRD campaign. The
188 calculation method can be found in Roberts et al. (2006).

189 Isoprene are mainly photo-oxidized through the reactions with OH radical in the
190 atmosphere and its primary first-generation reaction products are formaldehyde, MVK and
191 MACR (Apel et al., 2002) . The reaction processes of isoprene oxidized by OH radical are
192 mainly as follows:



196 where k_1 , k_2 , k_3 are the rate constants of the reactions. According to above reactions, the
197 relationship between MVK/Isoprene, MACR/Isoprene, (MVK+MACR)/Isoprene and the
198 reaction time Δt can be described as follows (Apel et al., 2002):

199
$$\frac{\text{MVK}}{\text{Isoprene}} = \frac{0.32k_1}{k_2 - k_1} (1 - \exp((k_1 - k_2)[\text{OH}]\Delta t)) \quad (\text{S11})$$

200
$$\frac{\text{MACR}}{\text{Isoprene}} = \frac{0.23k_1}{k_3 - k_1} (1 - \exp((k_1 - k_3)[\text{OH}]\Delta t)) \quad (\text{S12})$$

201
$$\frac{\text{MVK+MACR}}{\text{Isoprene}} = \frac{0.32k_1}{k_2 - k_1} (1 - \exp((k_1 - k_2)[\text{OH}]\Delta t)) + \frac{0.23k_1}{k_3 - k_1} (1 - \exp((k_1 - k_3)[\text{OH}]\Delta t)) \quad (\text{S13})$$

202 where $\frac{MVK+MACR}{Isoprene}$ can be derived from the measurements by ToF-MS. Then the OH exposure
203 ($[OH]\Delta t$) of isoprenoids can be obtaind from Eq. S13.

204 **5. Estimation of SOA production rate from individual precursors**

205 Here we calculated the SOA production rate associated with OH radicals for each SOA
206 precursors based on the diurnal variation of each species. Here, only the oxidation of OH
207 radicals is considered(Atkinson and Arey, 2003). The SOA production rate represents the
208 instant SOA production amount by oxidation reaction with atmospheric OH radical at a
209 certain time for a specific precursor, which can be characterized as follows:

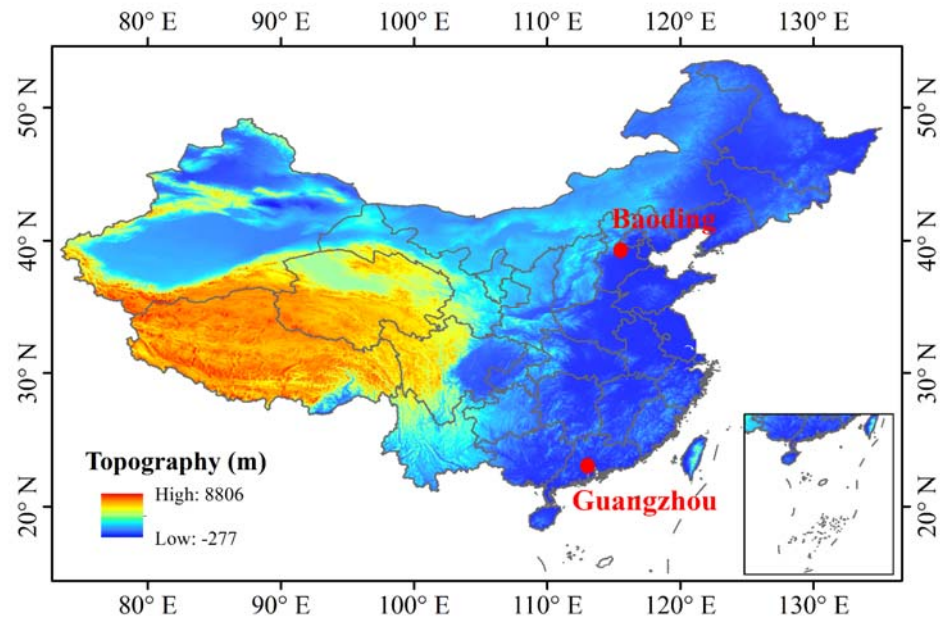
210 $[SOA_i]_t = [VOC_i]_t \times [OH]_t \times k_{VOC_i} \times Yield_i,$ (S14)

211 where for a given specific compound VOC_i , $[SOA_i]_t$ is the instant SOA production rate for
212 the species ($\mu\text{g m}^{-3} \text{ s}^{-1}$), $[VOC_i]_t$ is the concentration measured at time t ($\mu\text{g m}^{-3}$), $[OH]_t$ is
213 the OH concentration at time t (molecules cm^{-3}), k_{VOC_i} is the rate constant of VOC_i with the
214 OH radical ($\text{cm}^3 \text{ molecule}^{-1} \text{ s}^{-1}$) and $Yield_i$ is the SOA yield.

215 Based on equation (S14), SOA instant production for higher alkanes (C8-C20),
216 monoaromatics (benzene, toluene, C8 aromaics, C9 aromaics), naphthalenes (naphthalene,
217 methylnaphthalenes, dimethylnaphthalenes) and isoprenoids (isoprene, monoterpenes) were
218 calculated. The OH reaction rate constant of each compound was taken literature (Atkinson,
219 2003). SOA yield data used here for alkanes (Lim and Ziemann, 2009;Presto et al.,
220 2010b;Loza et al., 2014;Lamkaddam et al., 2017a), monoaromatics (Li et al., 2016;Tajuelo
221 et al., 2019;Ng et al., 2007), naphthalenes (Chan et al., 2009) and isoprenoids (Ahlberg et al.,
222 2017;Carlton et al., 2009;Edney et al., 2005;Kleindienst et al., 2006;Pandis et al., 1991) were
223 summarized from reported values in the literature, with the consideration on the influence of
224 organic aerosol concentration (Figure S20) to SOA yield (Figure S21-22). OH

225 concentrations are derived from an observation-constrained box model utilizing MCM
226 v3.3.1 as the chemical mechanisms(Wolfe et al., 2016).

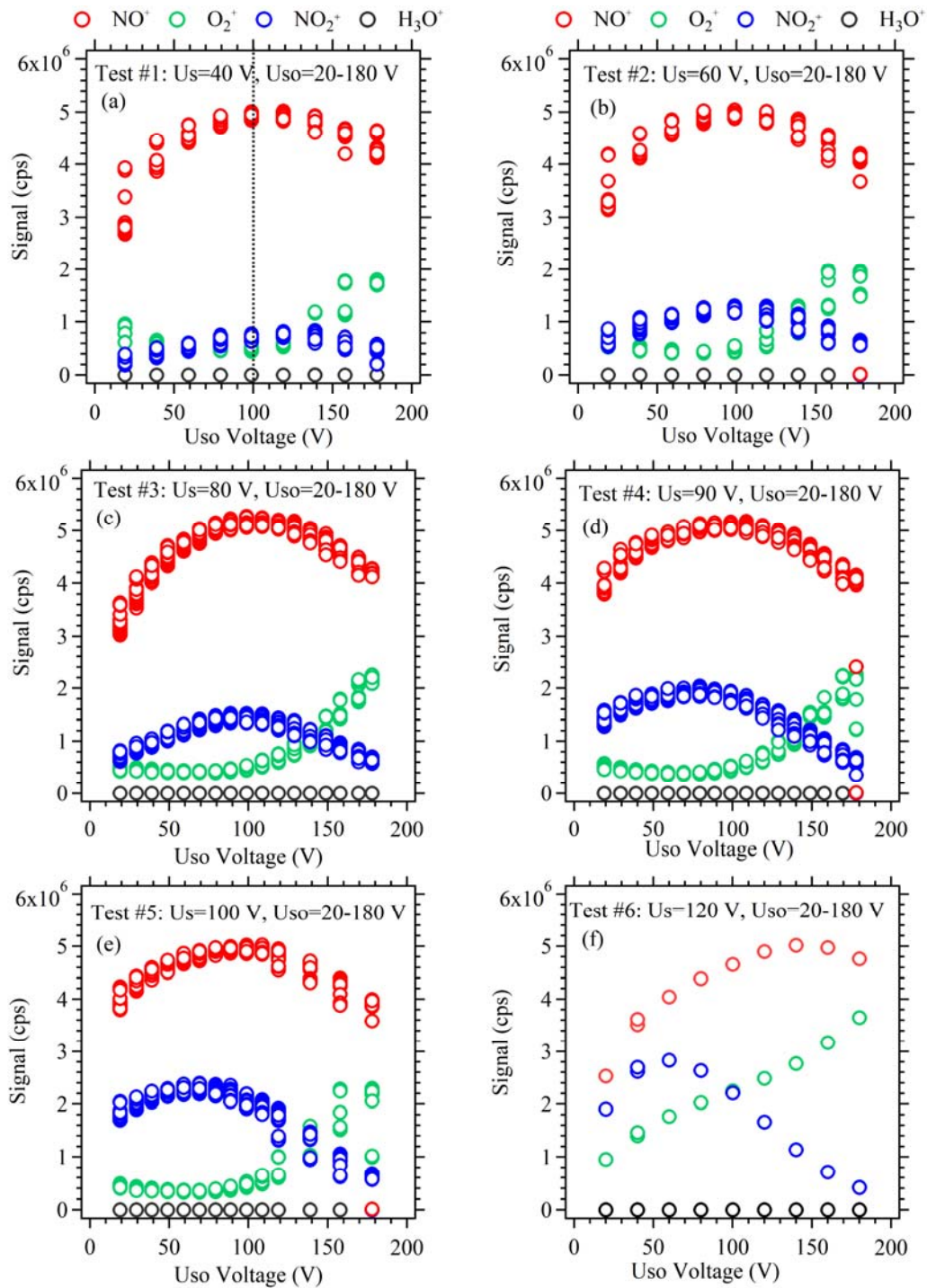
227 As shown in Figure S29, the total mean SOA production rate of higher alkanes (C8-C20)
228 is much higher compared to other VOCs classes, ~1.9 times of monoaromatics, ~7.8 times
229 of naphthalenes and ~2.4 times of isoprenoids at the urban site in PRD. At the rural site in
230 NCP, the total mean SOA production rate of higher alkanes (C8-C20) is comparable to
231 monoaromatics and slightly higher than that of naphthalenes and isoprenoids. Strong diurnal
232 variations are observed in both sites. In comparison with the rural site in NCP, SOA
233 production rates of VOCs are much higher at the urban cite in PRD. This is mainly due to
234 the higher OH concentrations (Figure S16) by strong solar radiation under high humidity
235 conditions in PRD during autumn, compared to dry and cold environment during the
236 measurements in NCP.



237

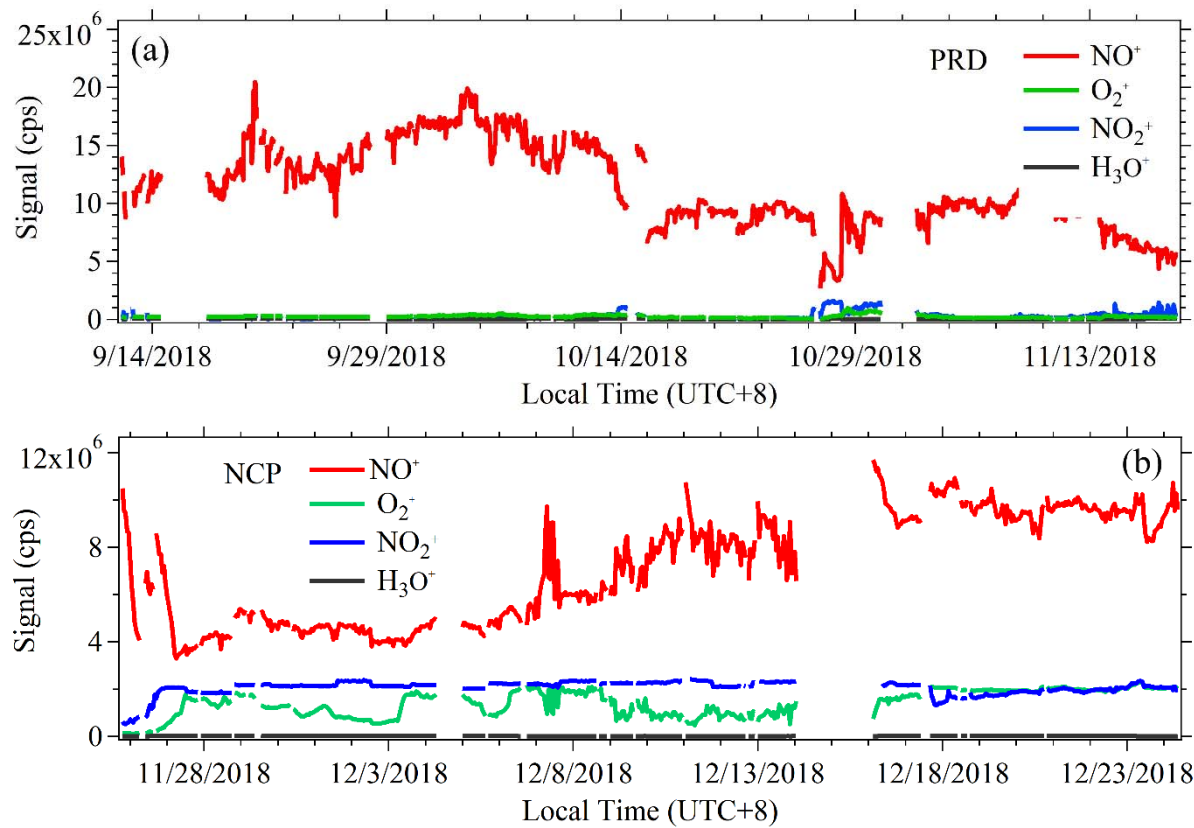
238 **Figure S1.** Sampling site locations of Guangzhou Campaign in PRD and Baoding Campaign
239 in NCP of China.

240



241

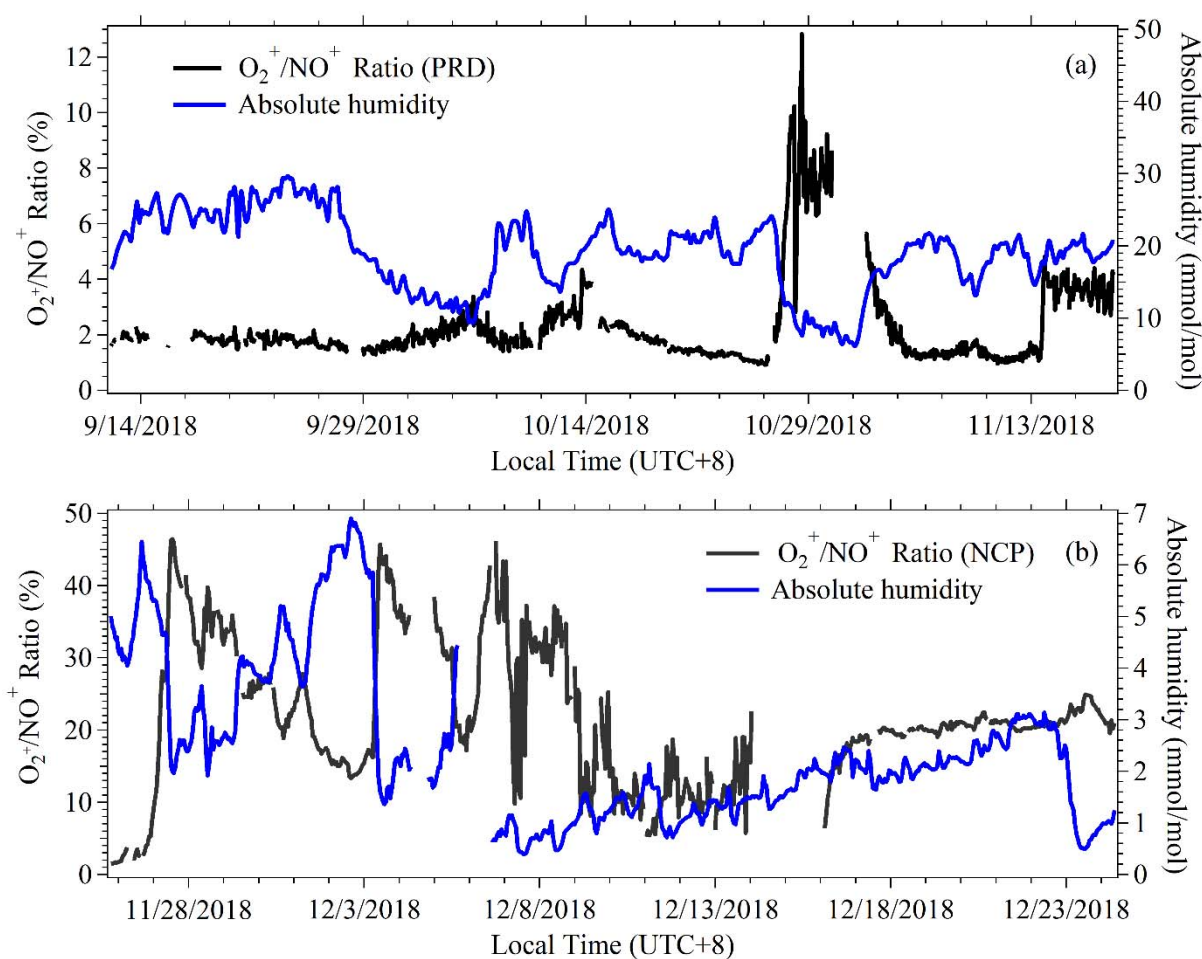
242 **Figure S2.** The variations of NO^+ , H_3O^+ , O_2^+ and NO_2^+ ions on the voltages of ion source
 243 (Us and Uso) for NO^+ PTR-ToF-MS. For each experiment, either Us or Uso is fixed at a
 244 voltage and the other was varied to explore the best setting for NO^+ PTR-ToF-MS. For
 245 example, test #1 in (a), we fix Us at 40 V and change Uso from 20 V to 180 V. The dashed
 246 line in (a) indicate the setting point in this study ($\text{Us}=40 \text{ V}$ and $\text{Uso}=100 \text{ V}$).



247

248 **Figure S3.** Time series of NO^+ , H_3O^+ , O_2^+ , NO_2^+ during the PRD (a) and the NCP (b)
249 campaigns, respectively.

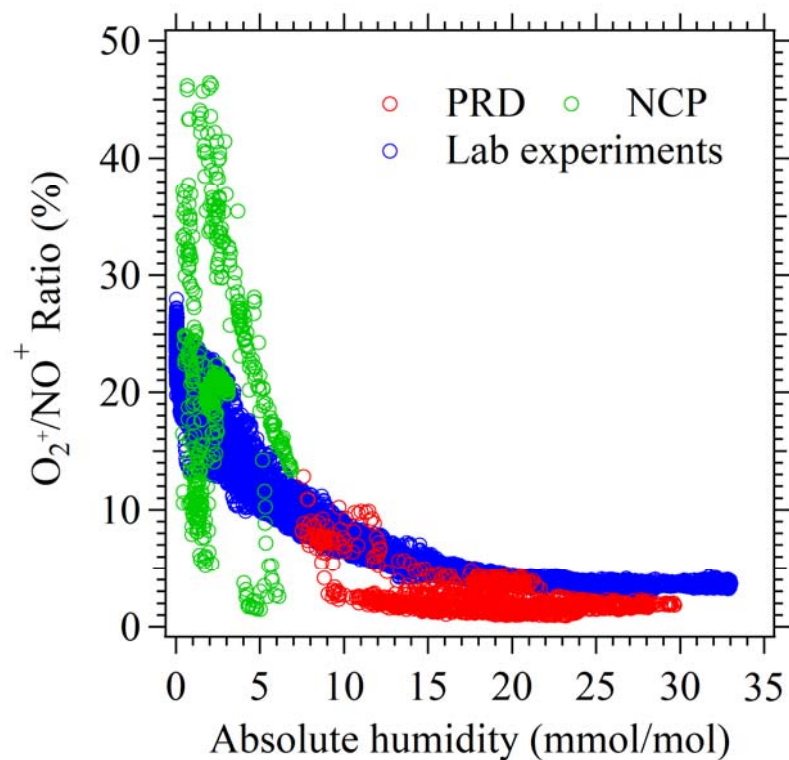
250



251

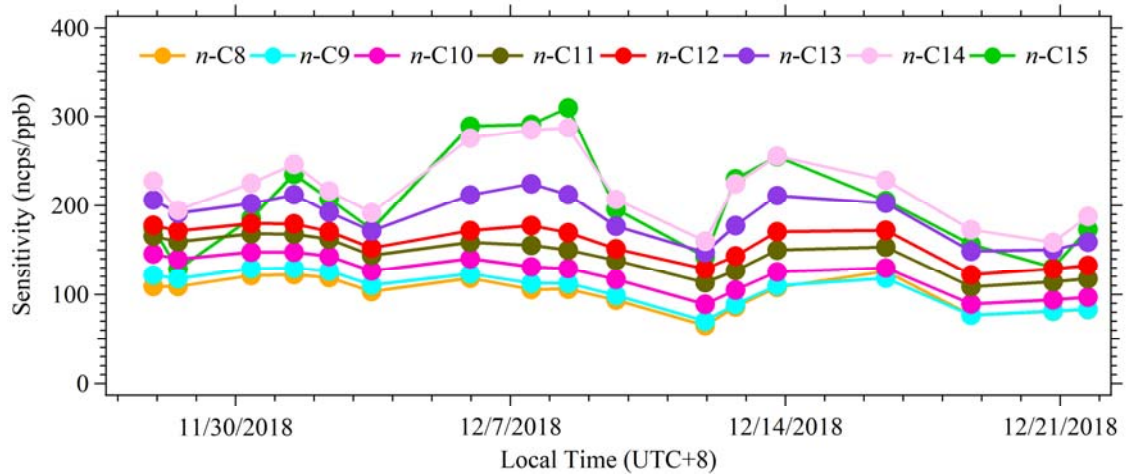
252 **Figure S4.** Time series of O_2^+ to NO^+ ratios and absolute humidity during the PRD **(a)** and
253 the NCP **(b)** campaigns, respectively.

254



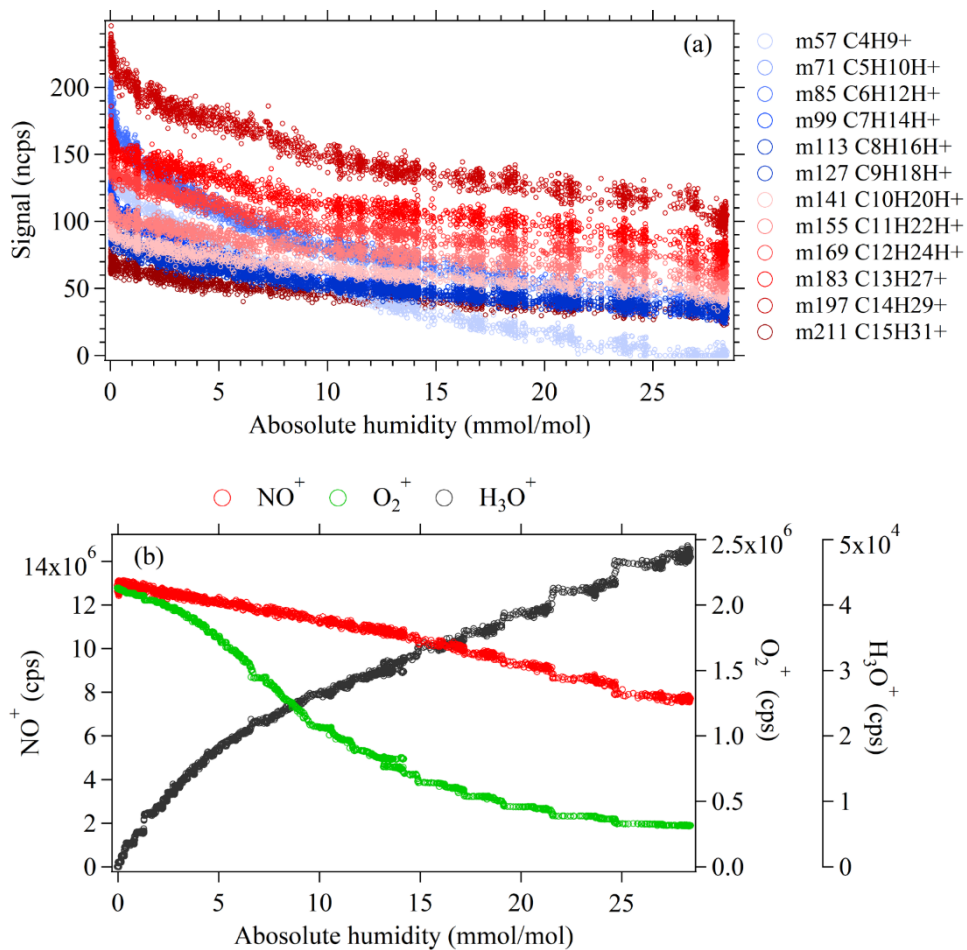
255

256 **Figure S5.** Humidity dependence of O_2^+ to NO^+ ratios during the lab experiment and the two
257 field campaigns.



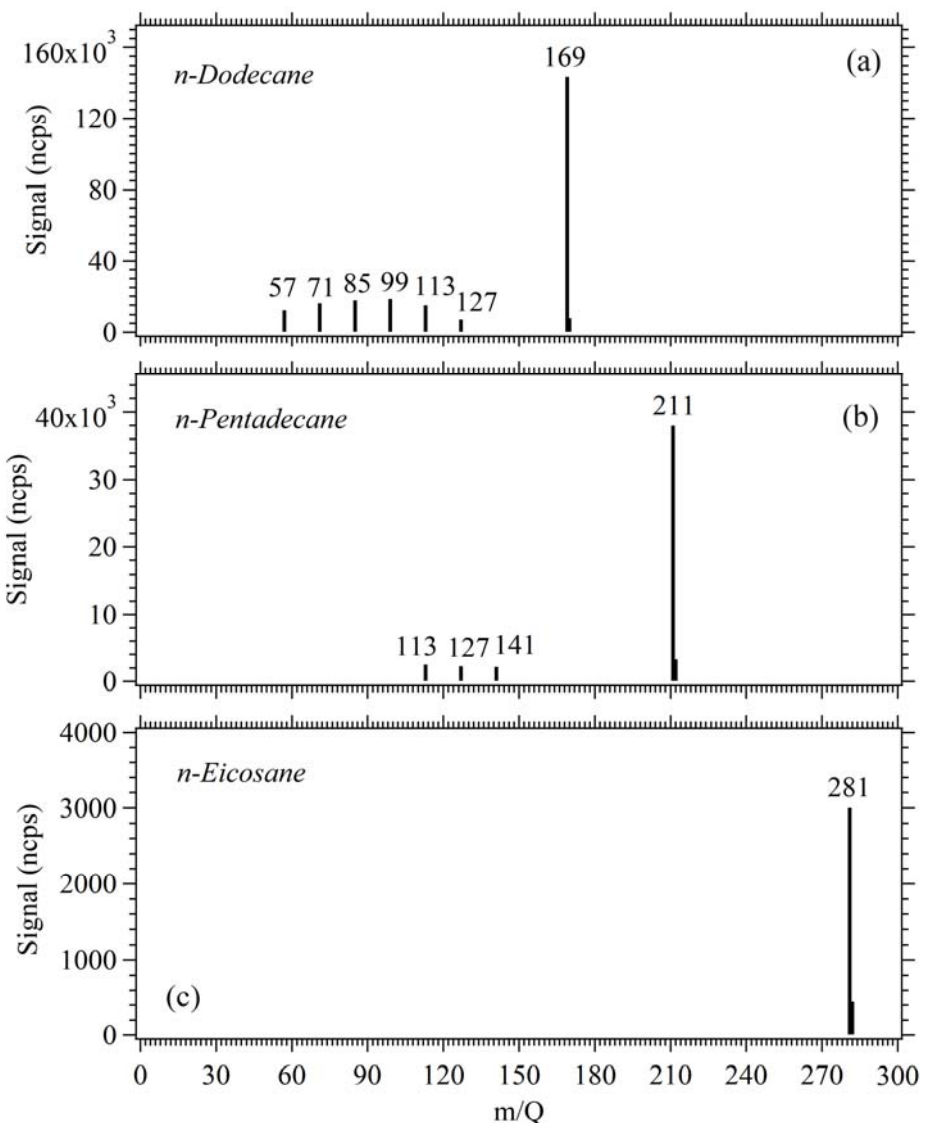
258

259 **Figure S6.** Calibration factors of C8-C15 *n*-alkanes under dry conditions (RH<1%) during
260 the two field campaigns.



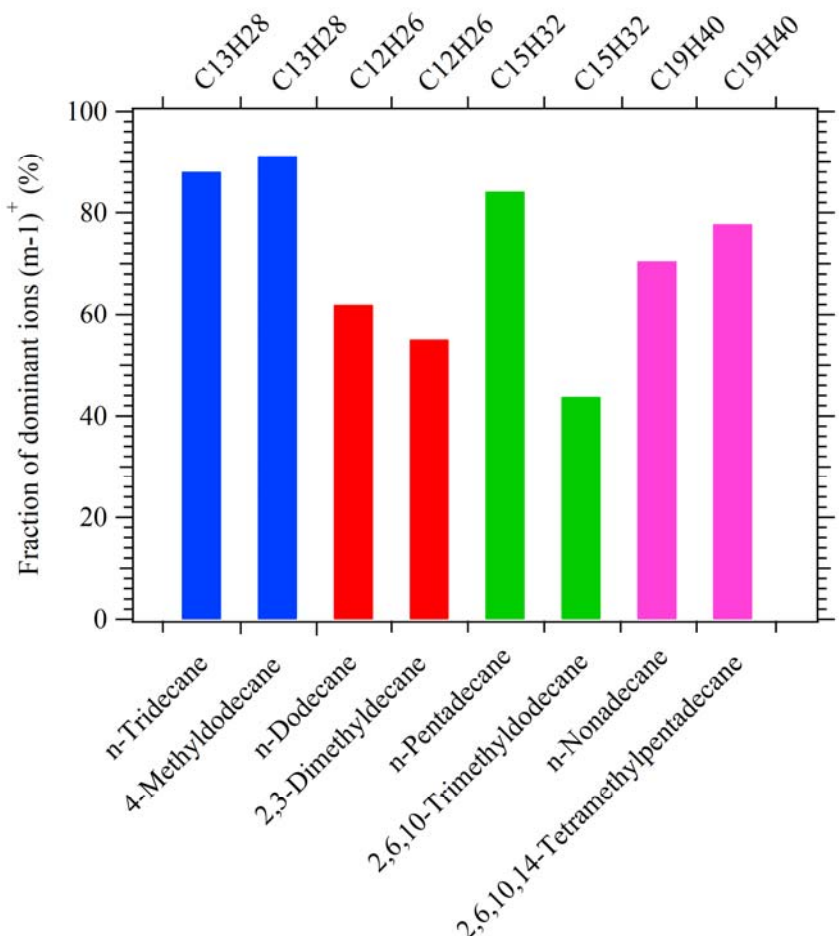
261

262 **Figure S7.** Humidity dependence of all product ions and the fragment ions for *n*-alkanes (C8-
 263 C15) **(a)**, and primary ions (NO⁺, O₂⁺, H₃O⁺) **(b)**.



264

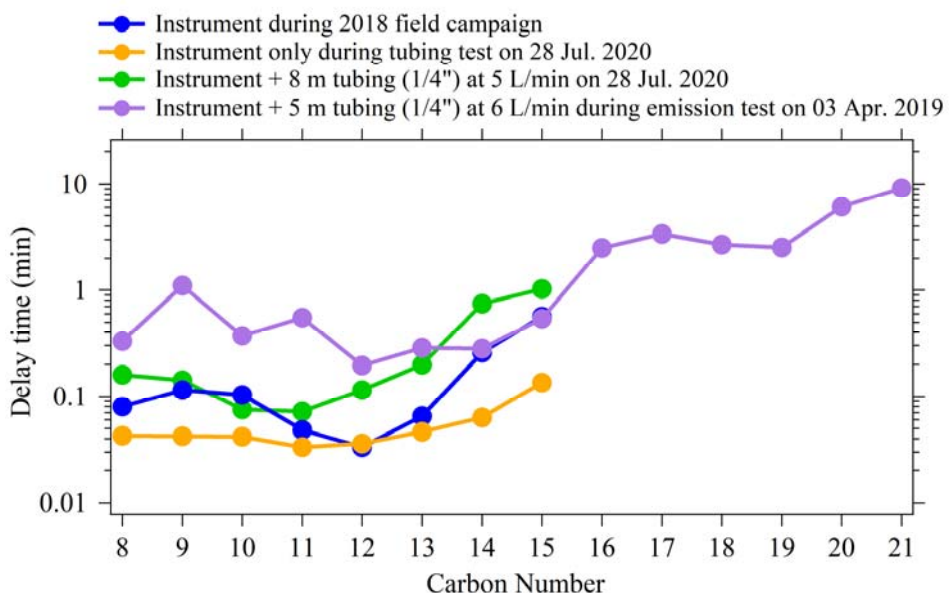
265 **Figure S8.** Mass spectra of the distributions of product ions from *n*-Dodecane **(a)**, *n*-
 266 Pentadecane **(b)** and *n*-Eicosane **(c)** with NO^+ PTR-ToF-MS. The signals of masses shown
 267 in the graph are the results after subtracting the isotopic signals during the high resolution
 268 peak fitting of the mass spectra.



269

270 **Figure S9.** Fraction of product ions ($m-1$)⁺ in the mass spectra of *n*-alkanes and their isomers
271 with different number of substituted methyl groups in NO⁺ PTR-ToF-MS.

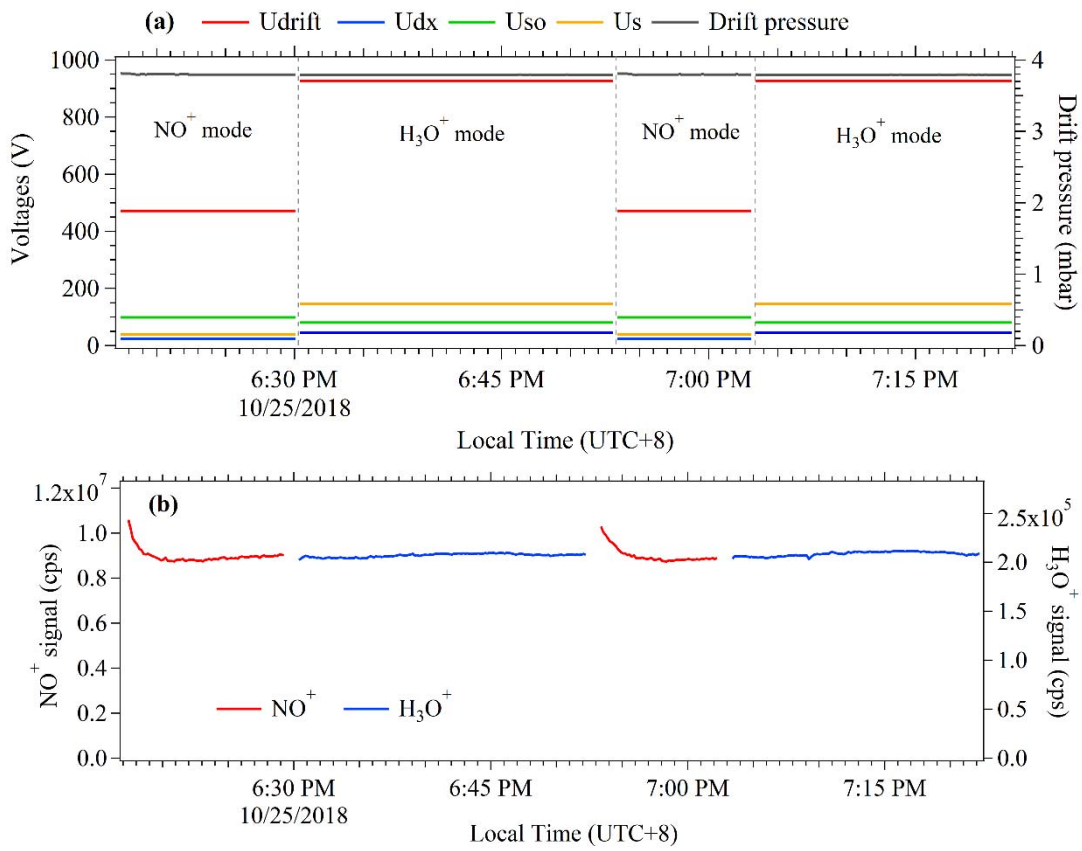
272



273

274 **Figure S10.** Delay times of higher alkanes for the field campaigns, emission source
 275 measurements and tubing losses test in the laboratory.

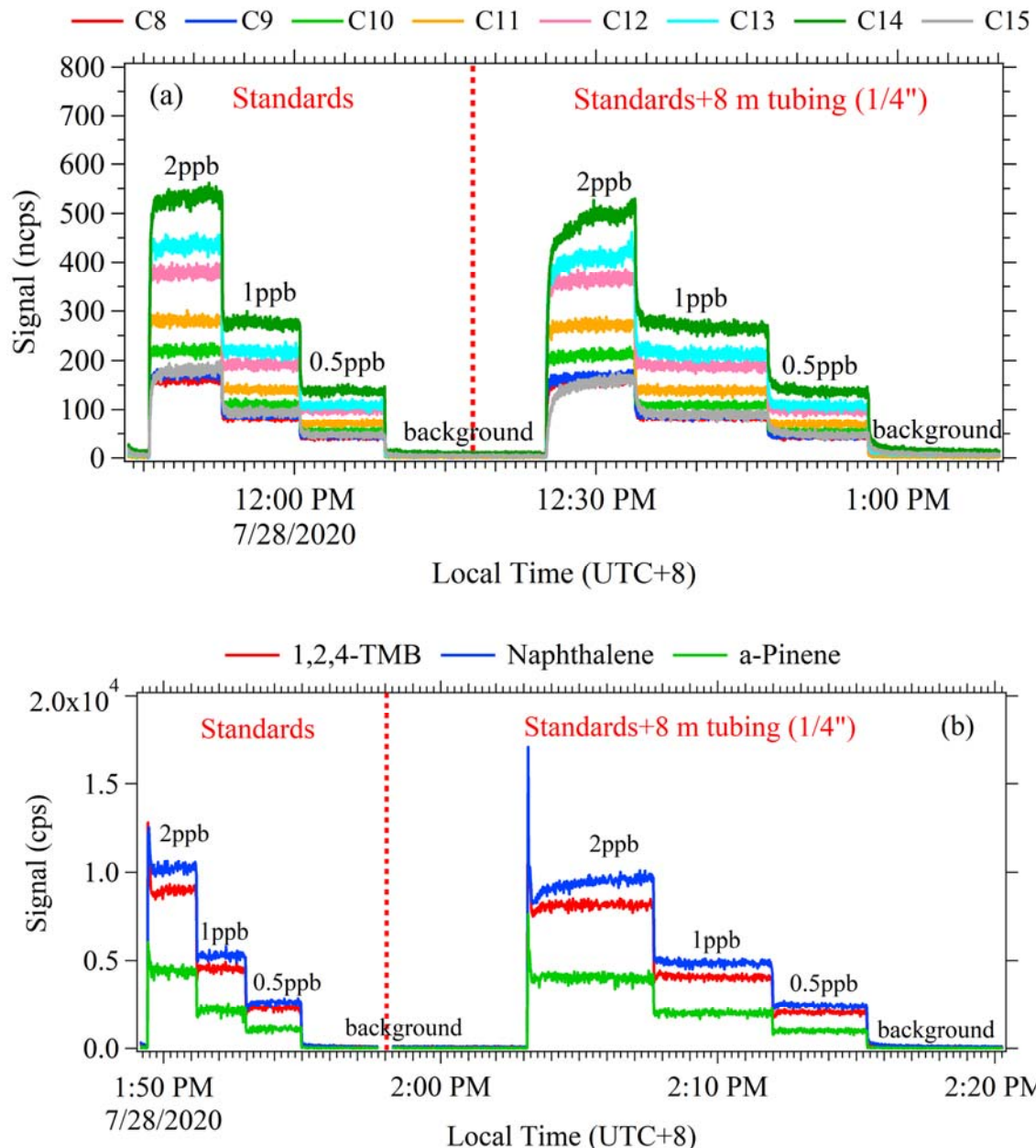
276



277

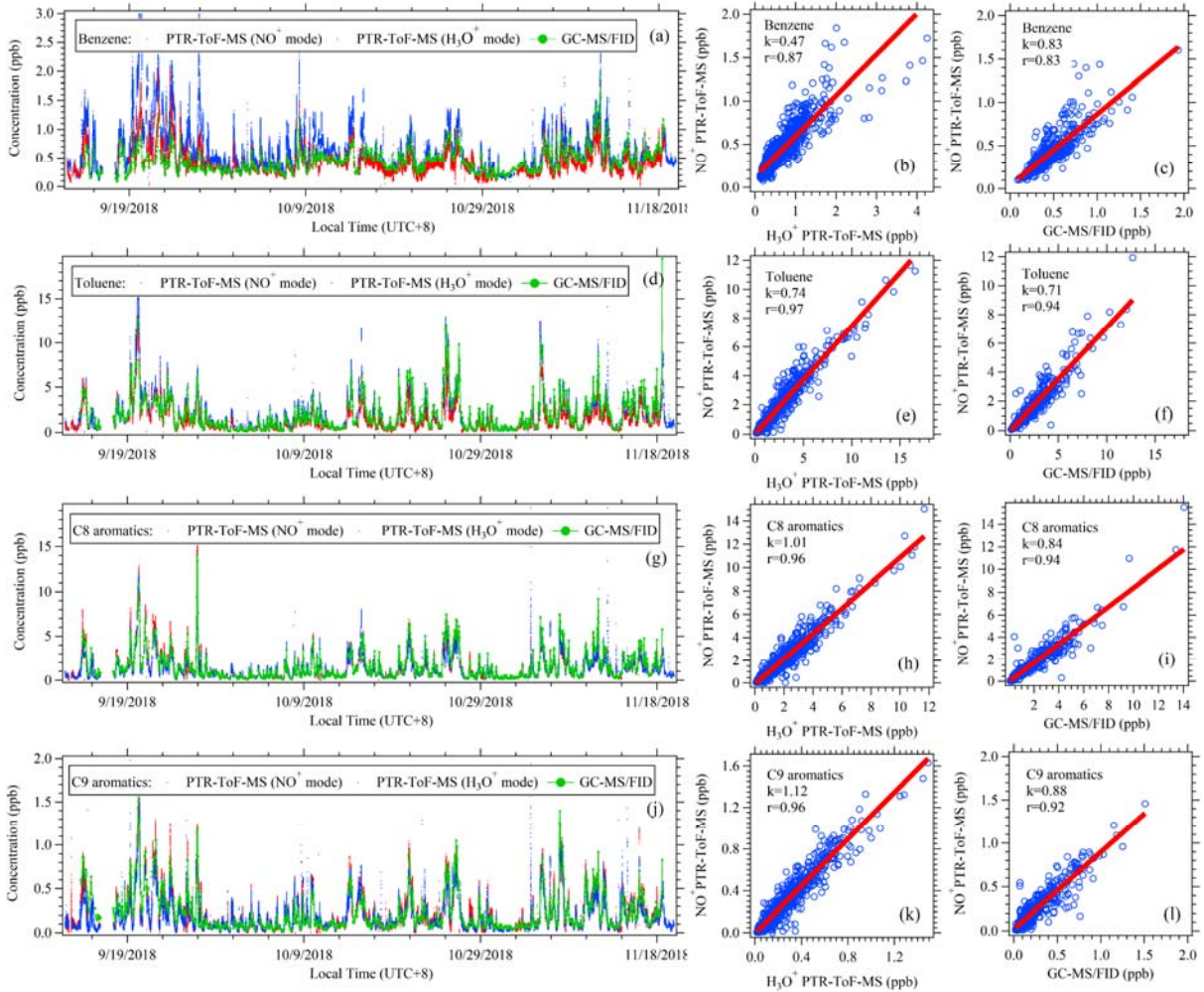
278 **Figure S11.** An example of voltages of ion source voltages (Us, Uso), drift tube (Udrift, Udx)
 279 and pressure of drift tube **(a)**, and the signal changes of primary ions **(b)** during automatical
 280 switching between NO⁺ mode and H₃O⁺ mode, respectively.

281



282 **Figure S12.** The tubing loss experiments of higher alkanes (*n*-C8-C15), 1,2,4-
 283 trimethylbenzene, α -pinene and naphthalene at room temperature using PTR-ToF-MS with an
 284 external pump at 5.0 L/min.
 285

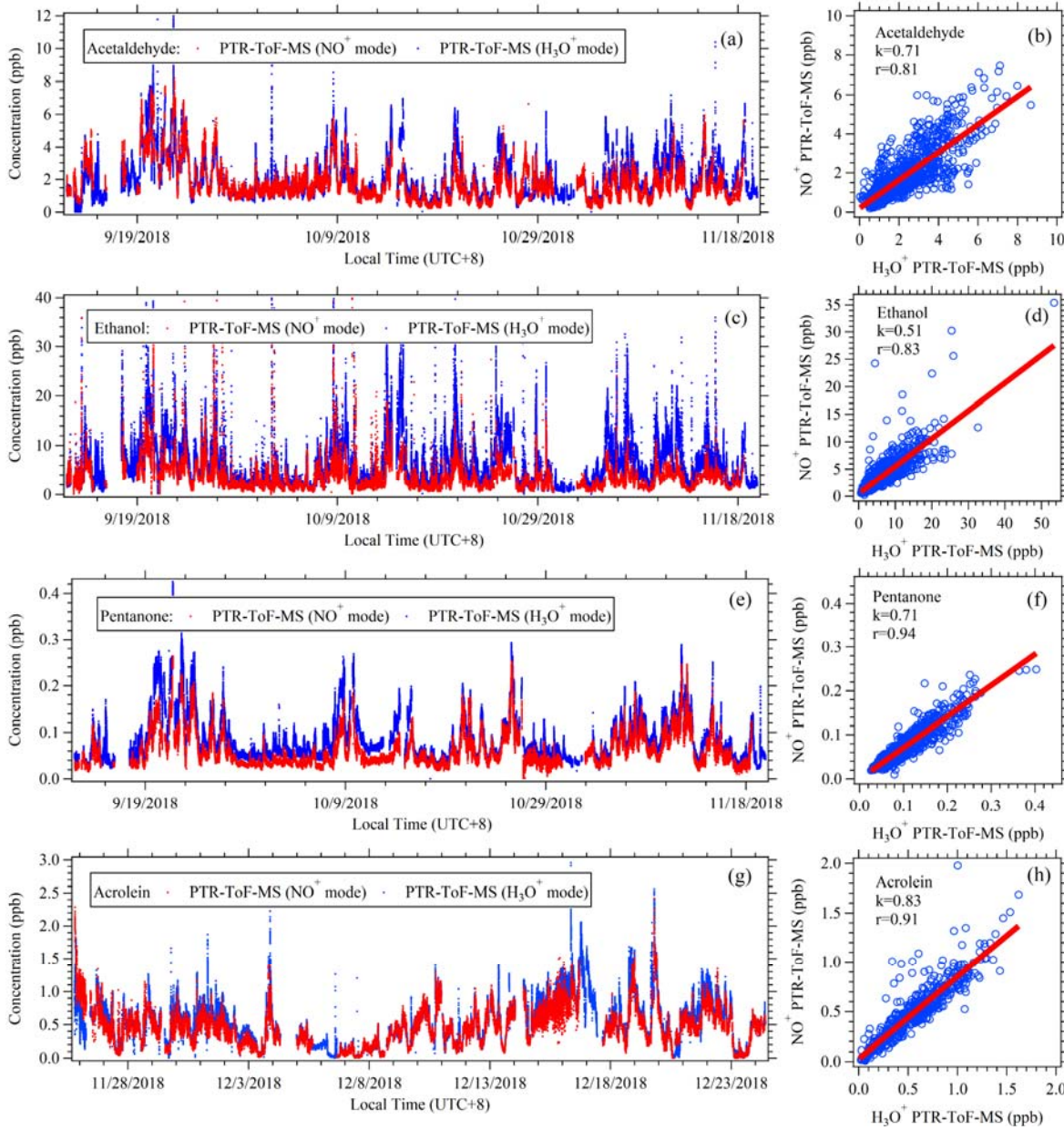
286



287

288 **Figure S13.** Comparisons of benzene, toluene, C8 aromatics and C9 aromatics measured by
 289 NO⁺ PTR-ToF-MS (red dots), H₃O⁺ PTR-ToF-MS (blue dots) and GC-MS/FID (green lines
 290 and dots) during the PRD campaign.

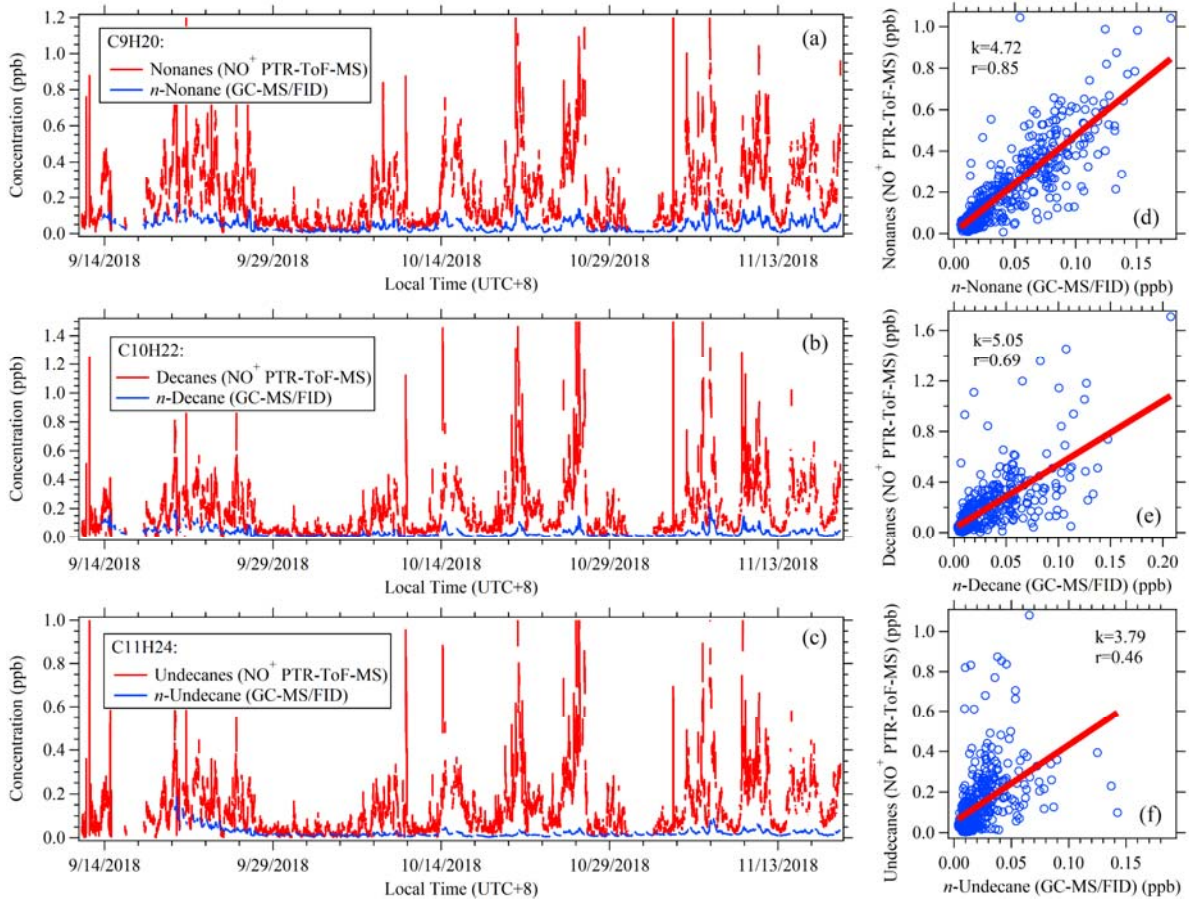
291



292

293 **Figure S14.** Comparisons of acetaldehyde, pentanone, ethanol and acrolein measured by
 294 NO⁺ PTR-ToF-MS (red dots) and H₃O⁺ PTR-ToF-MS (blue dots) during the PRD and NCP
 295 campaigns.

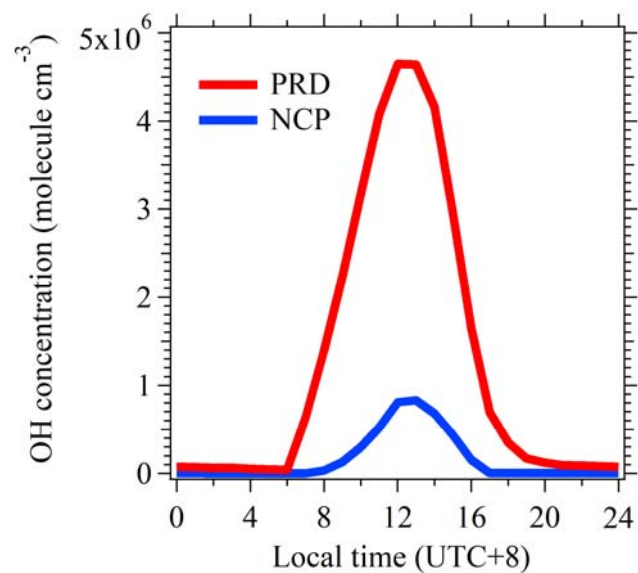
296



297

298 **Figure S15** Comparisons of C9-C11 alkanes measured by NO^+ PTR-ToF-MS and GC-
299 MS/FID during PRD campaign.

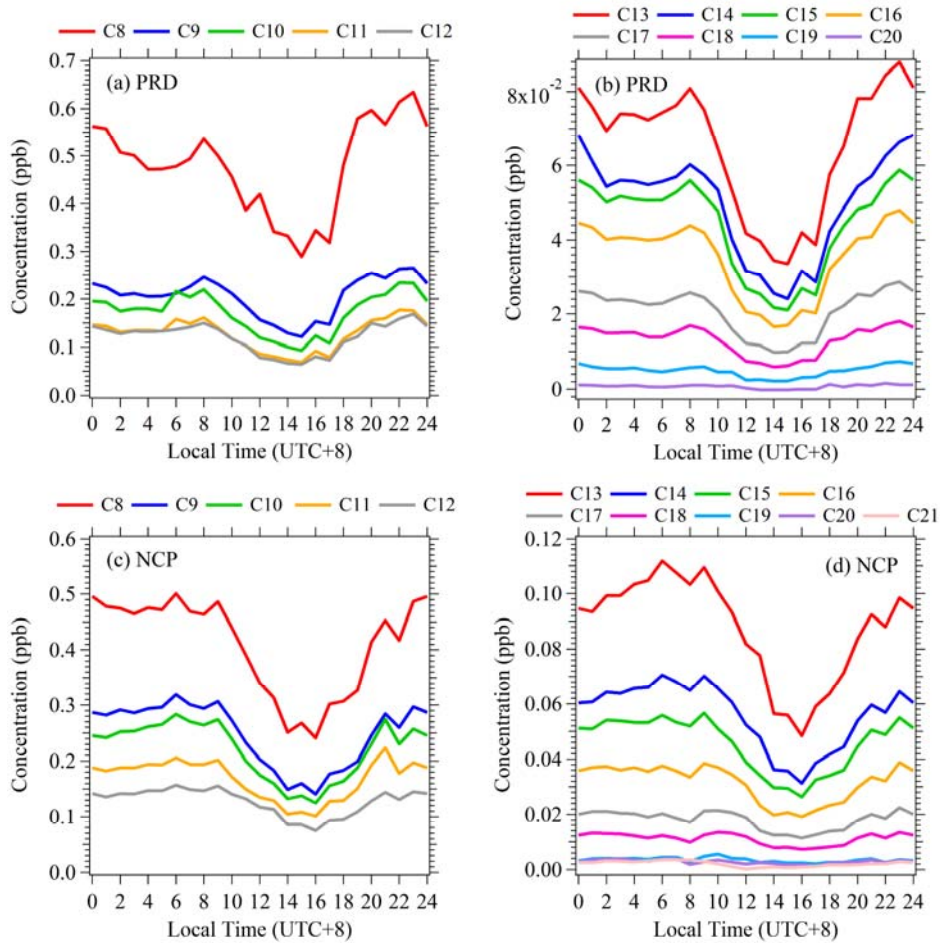
300



301

302 **Figure S16.** Diurnal variations of OH concentrations in PRD and NCP, respectively. OH
303 concentrations are derived from an observation-constrained box model utilizing MCM v3.3.1
304 as the chemical mechanisms(Wolfe et al., 2016).

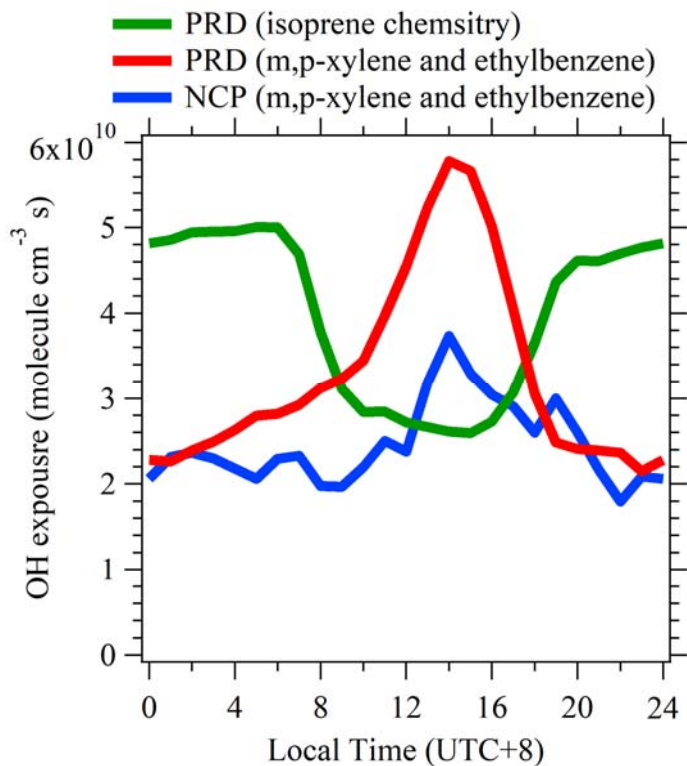
305



306

307 **Figure S17.** Similar diurnal profiles of C8-C21 alkanes during campaigns in PRD (a, b) and
 308 NCP (c, d).

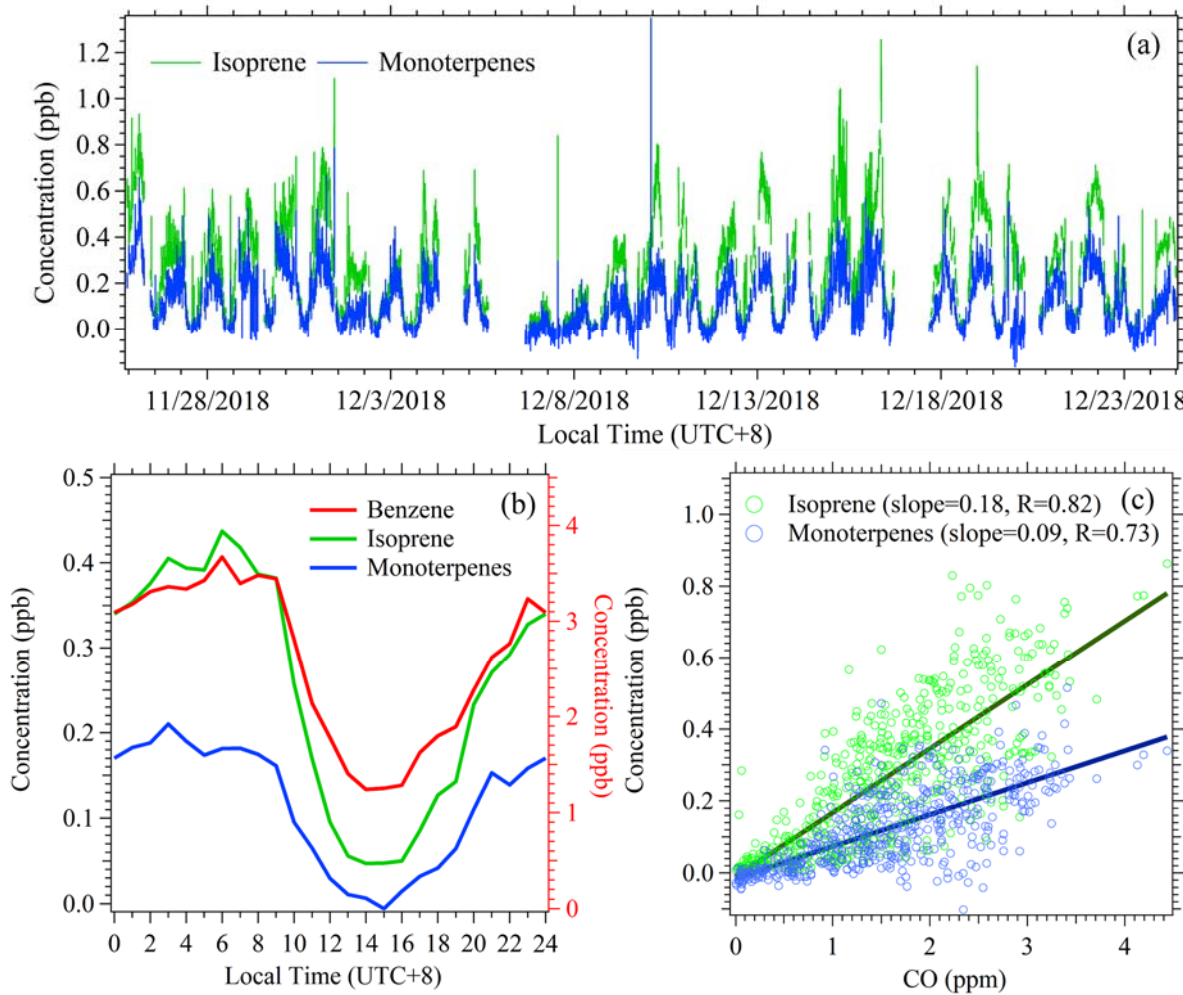
309



310

311 **Figure S18.** Comparisons of average diurnal variations of OH exposure calculated from the
 312 ratio of m+p-xylene and ethylbenzene for anthropogenic compounds in PRD and NCP and
 313 isoprene chemistry in PRD for biogenic compounds.

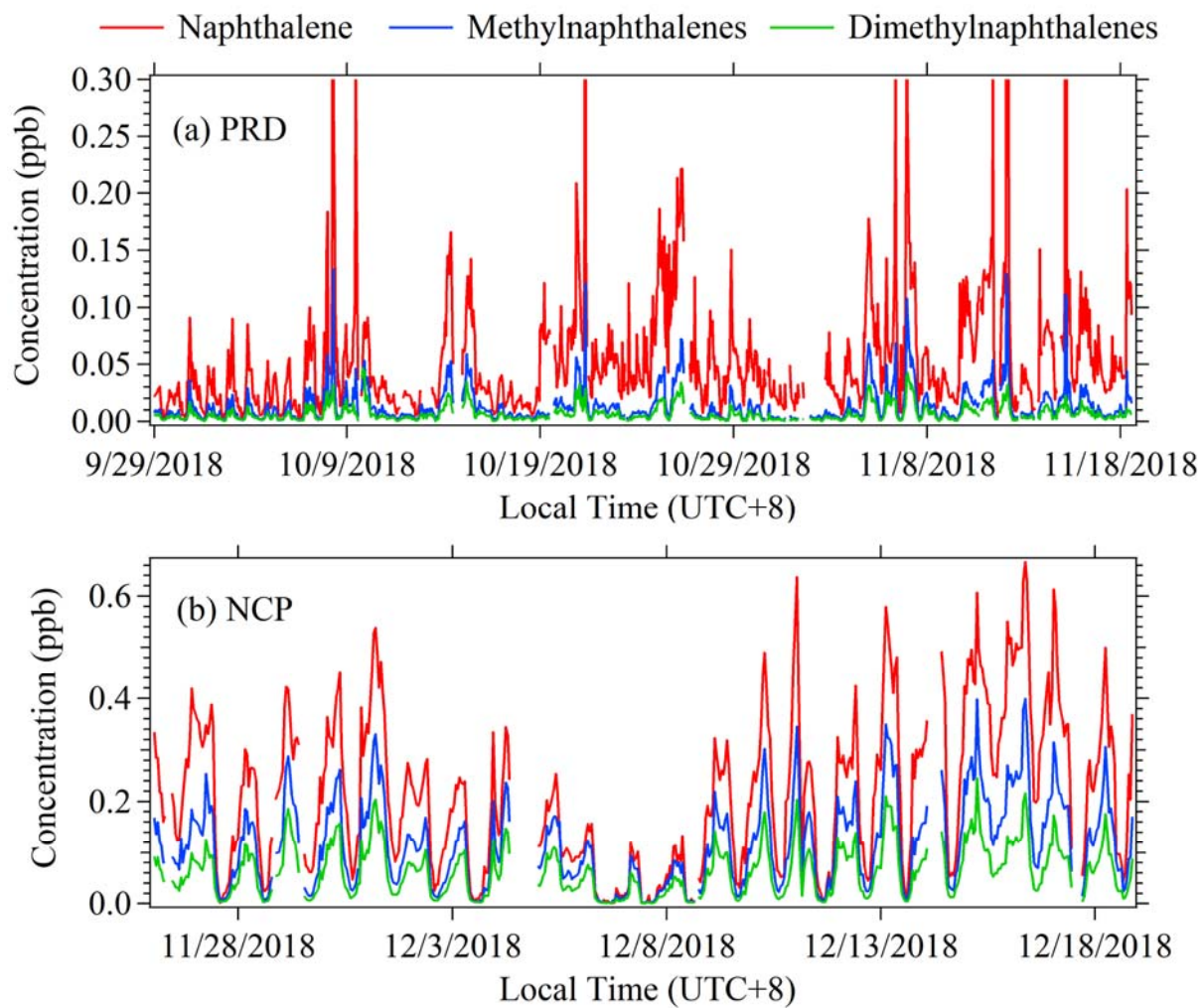
314



315

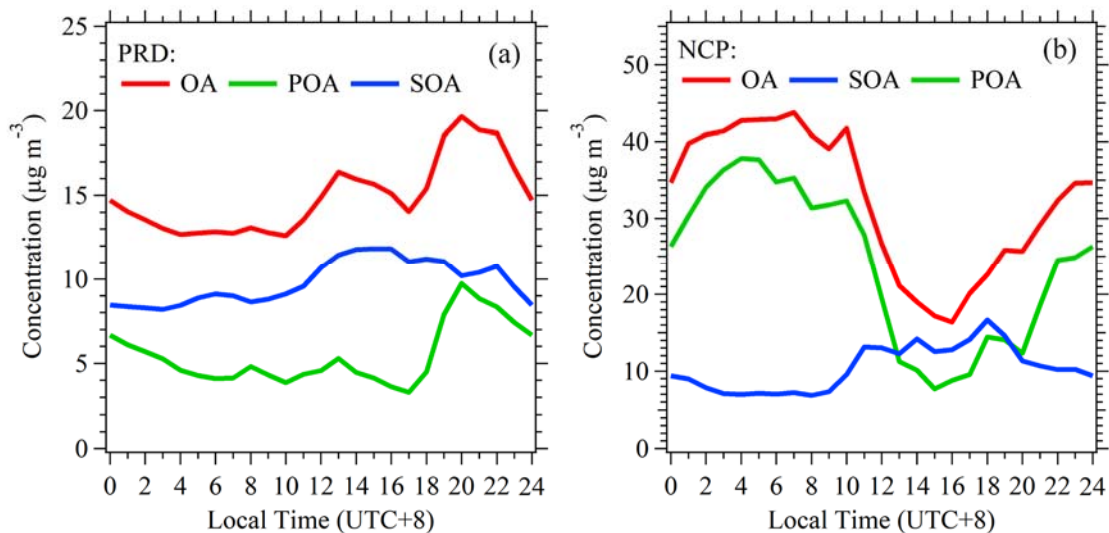
316 **Figure S19.** (a) Time series of isoprene and monoterpenes in NCP. (b) Diurnal variation of
 317 isoprene, monoterpenes and benzene in NCP. (c) Scatter plot of isoprene and monoterpenes
 318 versus CO in NCP.

319

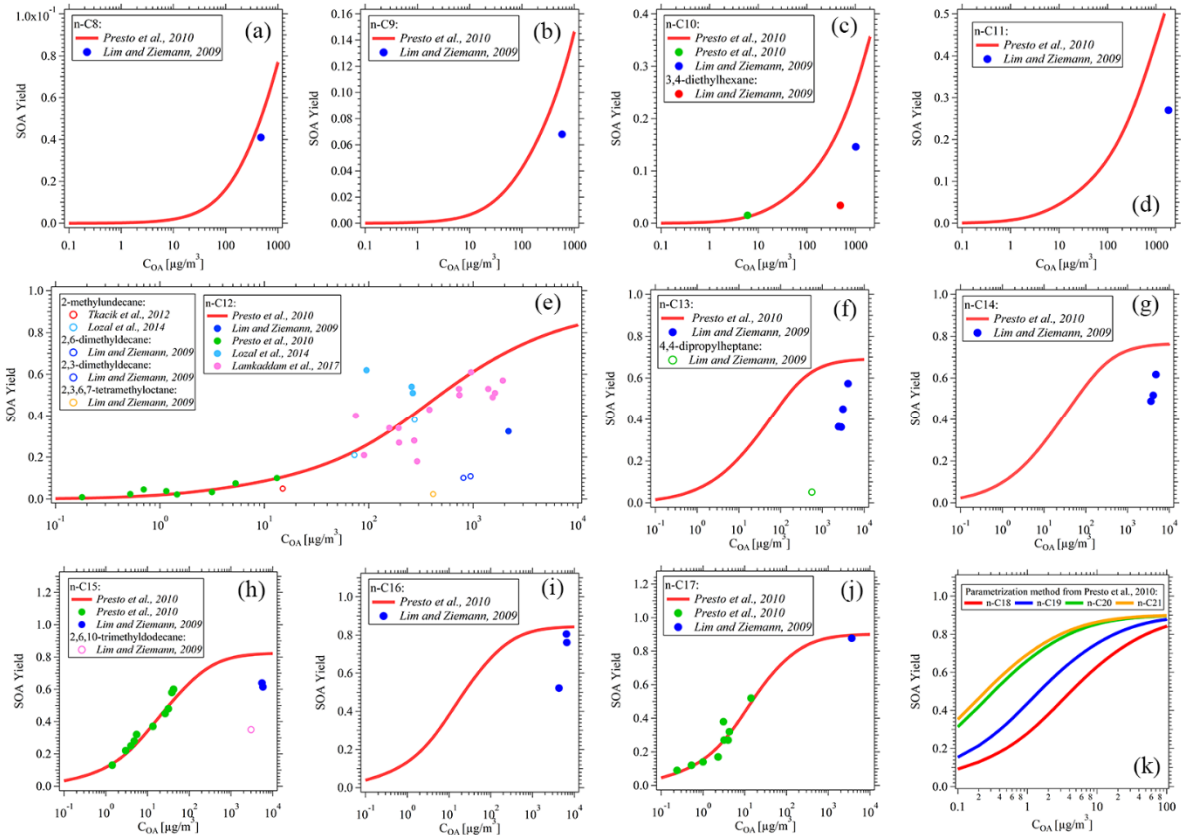


320

321 **Figure S20.** Time series of naphthalene, methylnaphthalenes, dimethylnaphthalenes in PRD
 322 (a) and NCP (b), respectively.

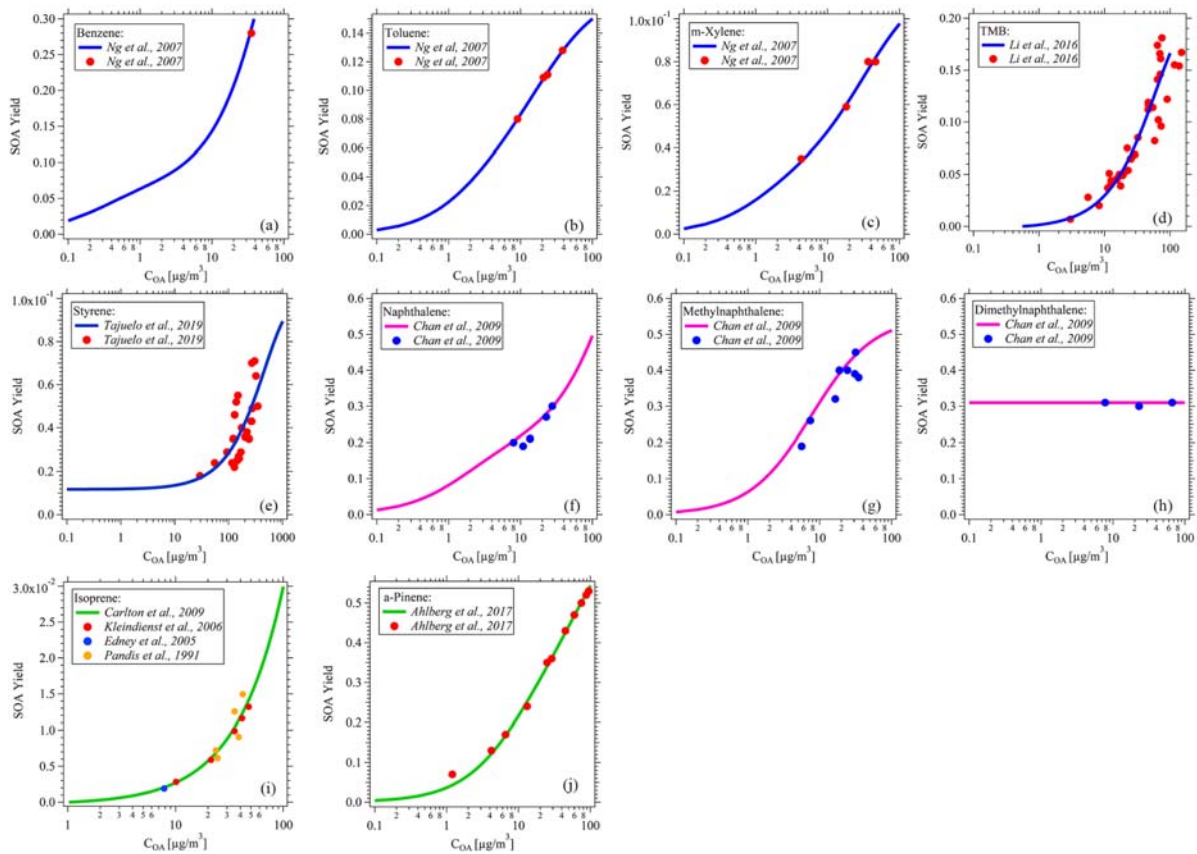


325 **Figure S21.** Diurnal variations of concentrations of organic aerosols (OA), secondary organic
 326 aerosols (SOA) and primary organic aerosols (POA) in PRD (a) and NCP (b). POA and SOA
 327 were determined by positive matrix factorization (PMF) analysis of OA measured by AMS.



328

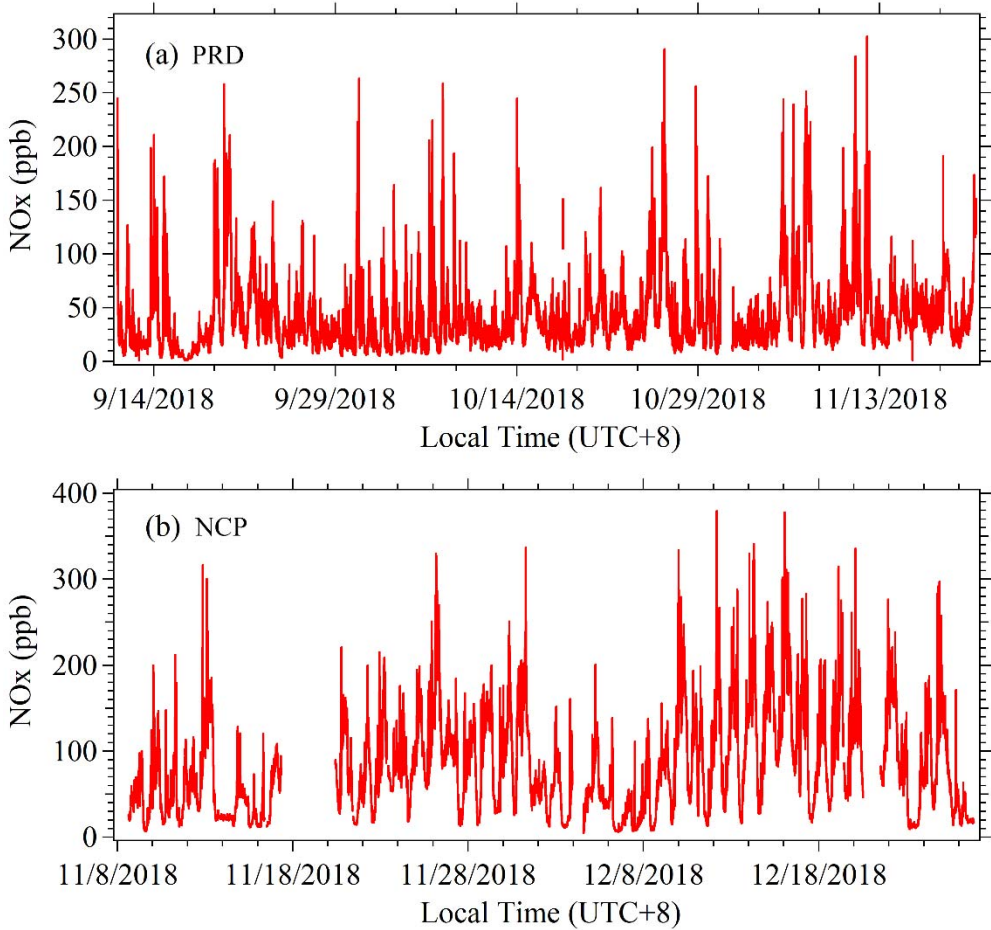
329 **Figure S22.** The reported SOA yields as a function of OA concentrations for higher alkanes
 330 (C8-C21 alkanes) (**a-k**) under high- NO_x condition from chamber studies(Lim and Ziemann,
 331 2009;Presto et al., 2010a;Tkacik et al., 2012;Loza et al., 2014;Lamkaddam et al., 2017b).



332

333 **Figure S23.** The reported SOA yields as a function of OA concentrations for monoaromatics
334 (benzene, toluene, m-xylene, 1,2,3-TMB/1,2,4-TMB/1,3,5-TMB, styrene)(Ng et al., 2007;Li
335 et al., 2016;Tajuelo et al., 2019) **(a-e)**, naphthalenes (naphthalene, methylnaphthalene,
336 dimethylnaphthalenes)(Chan et al., 2009) **(f-h)** and isoprenoids (isoprene and α -
337 pinene)(Carlton et al., 2009;Edney et al., 2005;Kleindienst et al., 2006;Pandis et al.,
338 1991;Ahlberg et al., 2017) **(i-j)** under high-NO_x condition from chamber studies.

339

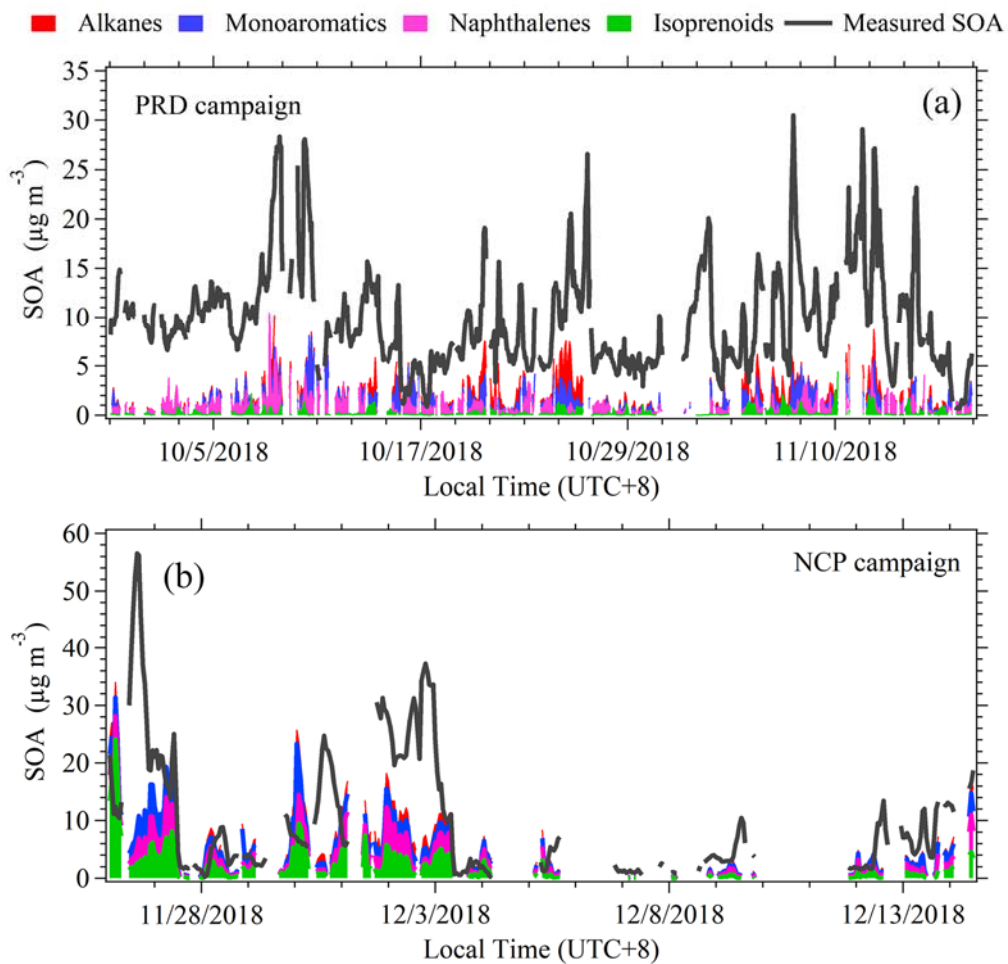


340

341 **Figure S24.** Time series of NO_x during the PRD (a) and the NCP (b) campaigns, respectively.

342

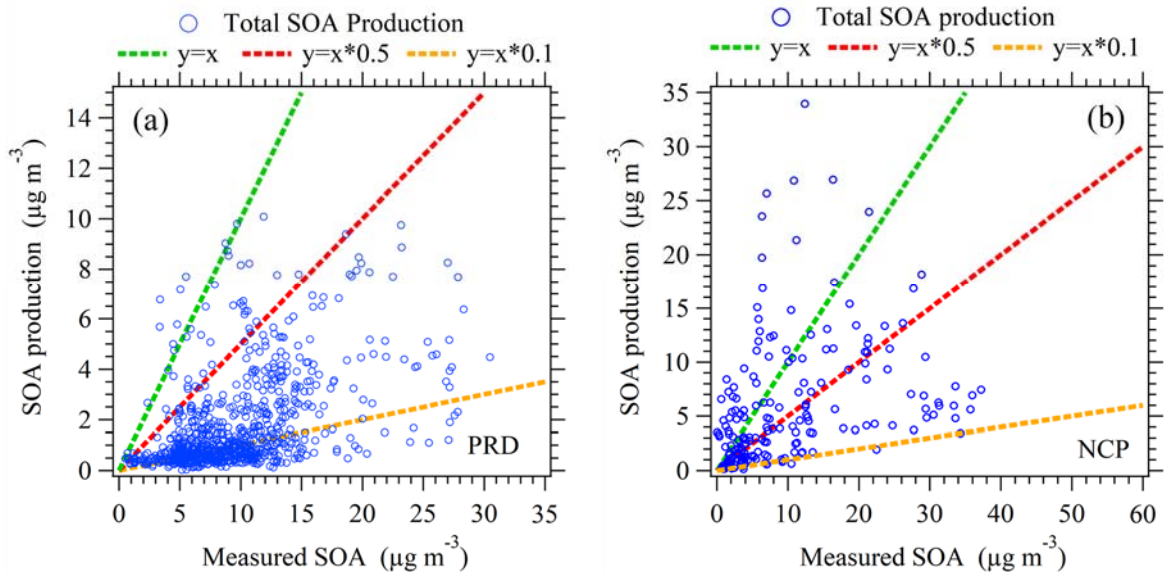
343



344

345 **Figure S25.** Time series of SOA produced from higher alkanes (C8-C21 alkanes),
 346 monoaromatics (benzene, toluene, C8 aromatics, C9 aromatics and styrene), naphthalenes
 347 (naphthalene, methylnaphthalenes, dimethylnaphthalenes) and isoprenoids (isoprene and
 348 monoterpenes) as well as the measured SOA concentrations in PRD (a) and NCP (b),
 349 respectively.

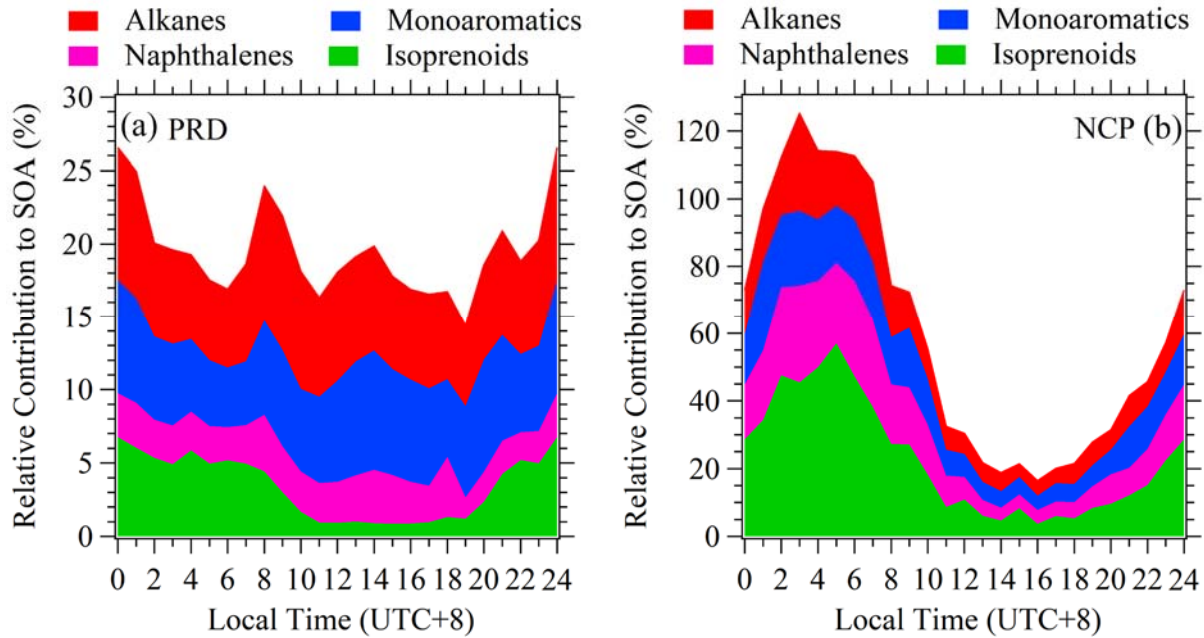
350



351

352 **Figure S26.** Scatter plots of total SOA production from higher alkanes (C8-C21 alkanes),
 353 monoaromatics (benzene, toluene, C8 aromatics, C9 aromatics and styrene), naphthalenes
 354 (naphthalene, methylnaphthalenes, dimethylnaphthalenes) and isoprenoids (isoprene and
 355 monoterpenes) versus measured SOA concentrations during the PRD campaign **(a)** and NCP
 356 campaign **(b)**.

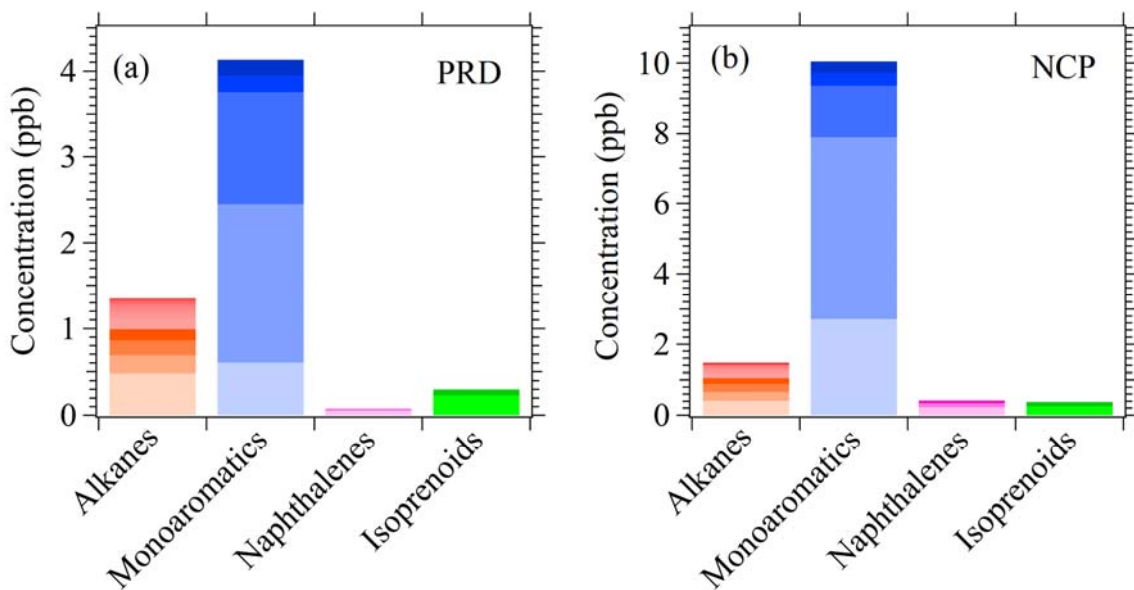
357



358

359 **Figure S27.** The relative contributions to measured SOA concentrations from higher alkanes
 360 (C8-C21 alkanes), monoaromatics (benzene, toluene, C8 aromatics, C9 aromatics and styrene),
 361 naphthalenes (naphthalene, methylnaphthalenes, dimethylnaphthalenes) and isoprenoids
 362 (isoprene and monoterpenes) in PRD **(a)** and NCP **(b)**.

363

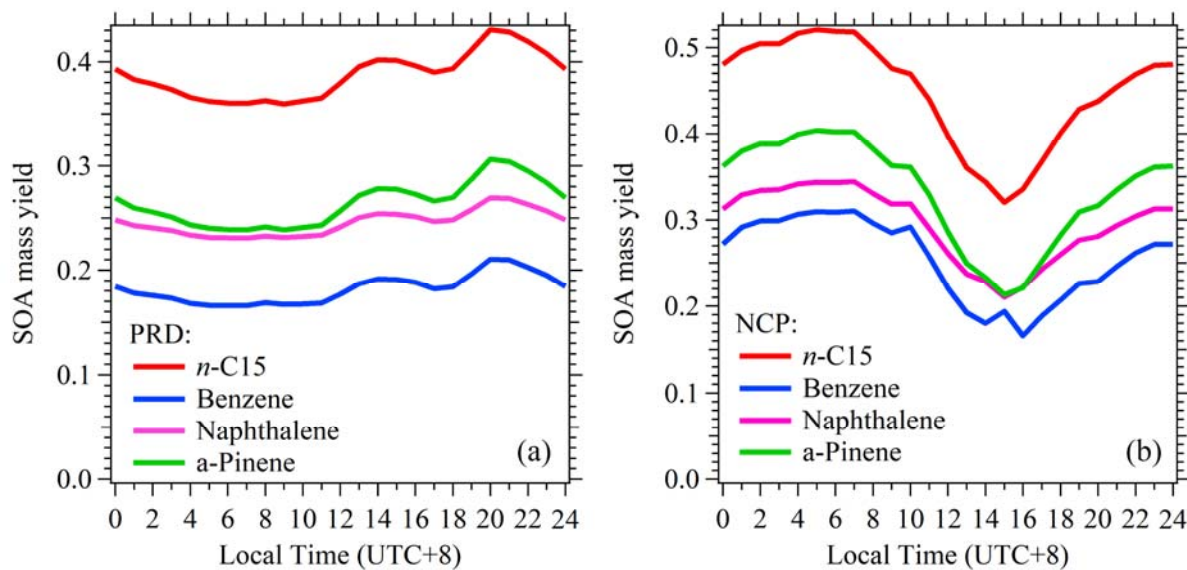


364

365 **Figure S28.** The average concentrations from higher alkanes (C8-C21 alkanes),
 366 monoaromatics (benzene, toluene, C8 aromatics, C9 aromatics and styrene), naphthalenes
 367 (naphthalene, methylnaphthalenes, dimethylnaphthalenes) and isoprenoids (isoprene and
 368 monoterpenes) in PRD **(a)** and NCP **(b)**, respectively.

369

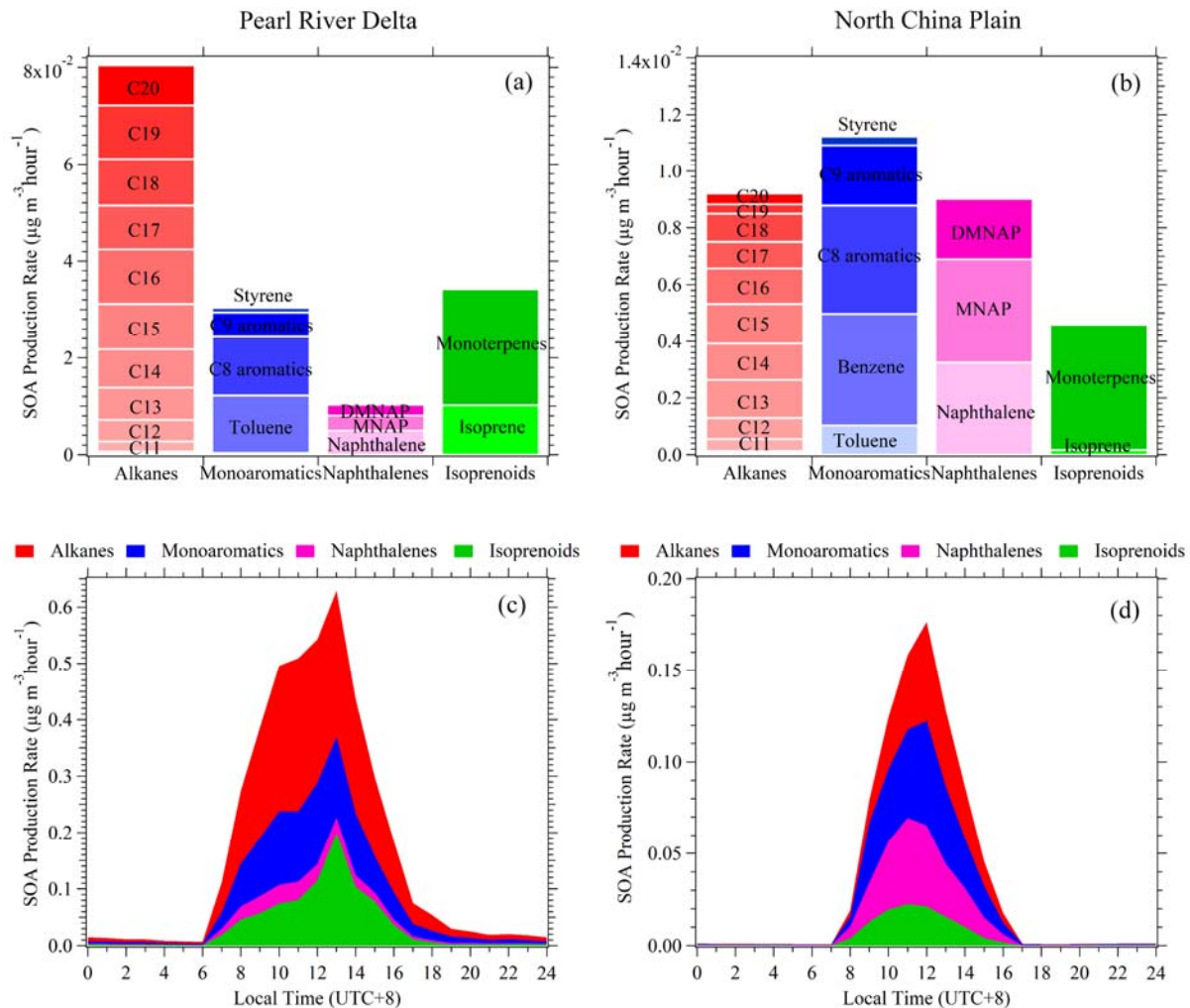
370



371

372 **Figure S29.** Diurnal variations of SOA yields of *n*-C15 alkane, benzene, naphthalene and α -
 373 pinene in PRD **(a)** and NCP **(b)**.

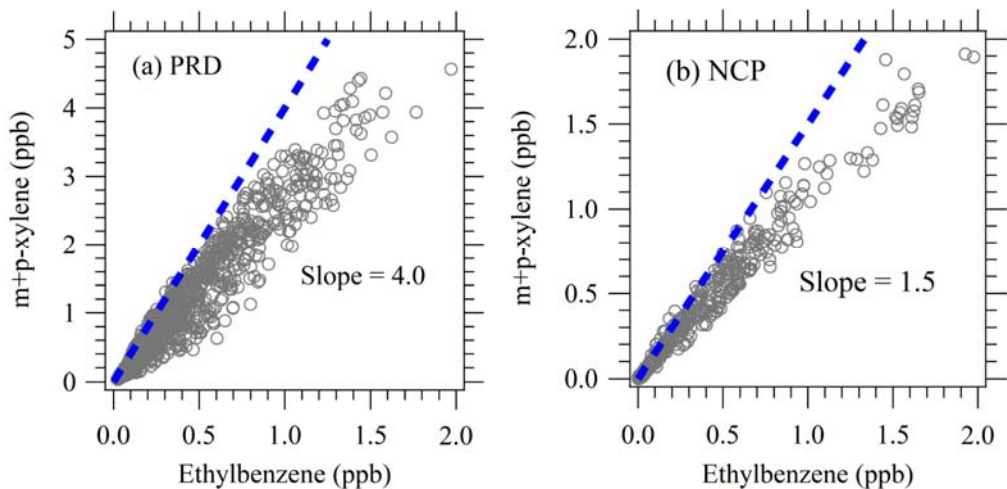
374



375

376 **Figure S30.** The mean SOA production rates of higher alkanes (C8-C20 alkanes),
377 monoaromatics (benzene, toluene, C8 aromatics, C9 aromatics and styrene), naphthalenes
378 (naphthalene, methylnaphthalenes, dimethylnaphthalenes) and isoprenoids (isoprene and
379 monoterpenes) and their hourly diurnal variations in PRD (a) and NCP (b). Diurnal variations
380 of alkanes, monoaromatics, naphthalenes and isoprenoids in PRD (c) and NCP (d).

381



382

383 **Figure S31.** Correlation of $m+p$ -xylene with ethylbenzene in PRD (a) and NCP (b). The
 384 dashed lines in both graphs indicate the estimated initial mission ratio of $m+p$ -
 385 xylene/ethylbenzene.

386

387 **Table S1.** The settings of the voltages of ion source voltages (Us, Uso), drift tube (Udrift, Udx)
388 and pressure of drift tube (pDrift) during automatical switching between NO⁺ mode and H₃O⁺
389 mode, respectively.

Setting	NO ⁺ mode	H ₃ O ⁺ mode
Us	40 V	150 V
Uso	100 V	80 V
Udrift	470 V	920 V
Udx	23.5 V	46 V
pDrift	3.8 mbar	3.8 mbar

390

391 **Table S2.** Fractions of *n*-alkanes in higher alkanes with same formulas derived from this study,
 392 ambient air in Los Angeles, Bakersfield, Caldecott Tunnel and in vehicle exhausts.

Carbon Number	Fraction of <i>n</i> -alkanes in higher alkanes with same formulas					
	PRD ^a	Los Angeles ^b	Bakersfield ^b	Caldecott Tunnel ^c	Diese exhaust ^d	Liquid gasoline exhaust ^d
8	10.82	/	/	/	37.04	5.39
9	21.48	/	/	/	51.22	7.71
10	17.56	/	/	/	23.81	8.81
11	17.81	/	/	/	20.91	10.88
12	/	/	/	/	22.54	29.82
13	/	/	/	/	21.98	/
14	/	/	/	/	19.84	5.41
15	/	/	/	/	22.86	40
16	/	/	/	/	25.44	/
17	/	/	/	/	32.16	/
18	/	/	/	/	28.57	/
19	/	/	/	/	20.83	/
20	/	34.78	24.85	/	20.87	/
21	/	53.16	12.47	/	24.82	/
22	/	42.85	9.11	/	25.51	/
23	/	40.24	8.14	58.82	21.05	/
24	/	21.85	6.92	34.62	24.44	/
25	/	27.17	27.87	32.35	60	/
26	/	/	/	25	/	/
27	/	/	/	27.03	/	/
28	/	/	/	38.64	/	/
29	/	/	/	29.63	/	/
30	/	/	/	23.53	/	/

393 ^a:This work; ^b: Chan et al. (2013); ^c: Worton et al. (2014); ^d: Gentner et al. (2012)

394

395 **Table S3.** The calculated average SOA yields of higher alkanes in PRD and NCP.

396	Compounds	Formula	Average SOA	Average SOA
397	Octane	C ₈ H ₁₈	0.003±0.002	0.006±0.004
	Nonane	C ₉ H ₂₀	0.010±0.005	0.017±0.010
	Decane	C ₁₀ H ₂₂	0.026±0.012	0.040±0.021
	Undecane	C ₁₁ H ₂₄	0.058±0.020	0.080±0.036
	Dodecane	C ₁₂ H ₂₆	0.106±0.032	0.142±0.059
	Tridecane	C ₁₃ H ₂₈	0.249±0.061	0.305±0.103
	Tetradecane	C ₁₄ H ₃₀	0.329±0.070	0.388±0.118
	Pentadecane	C ₁₅ H ₃₂	0.386±0.081	0.450±0.135
	Hexadecane	C ₁₆ H ₃₄	0.428±0.086	0.492±0.141
	Heptadecane	C ₁₇ H ₃₆	0.488±0.096	0.556±0.156
	Octadecane	C ₁₈ H ₃₈	0.664±0.079	0.704±0.139
	Nonadecane	C ₁₉ H ₄₀	0.773±0.056	0.792±0.105
	Eicosane	C ₂₀ H ₄₂	0.860±0.025	0.863±0.054
	Heneicosane	C ₂₁ H ₄₄	0.877±0.025	0.870±0.046

398 **Table S4.** Average biases in SOA yields due to vapour wall losses for various VOCs under
399 high-NO_x conditions from Zhang et al. (2014).

VOC	R _{wall}
Benzene	1.25±0.1
Toluene	1.13±0.06
m-xylene	1.2±0.1
Naphthalene	1.2±0.1
Isoprene	2.2±0.5
α-pinene	1.3±0.1
n-dodecane	1.16±0.08
2-methylundecane	1.4±0.2

400

401 **References**

- 402 Ahlberg, E., Falk, J., Eriksson, A., Holst, T., Brune, W. H., Kristensson, A., Roldin, P., and
403 Svenningsson, B.: Secondary organic aerosol from VOC mixtures in an oxidation flow reactor,
404 Atmospheric Environment, 161, 210-220, 10.1016/j.atmosenv.2017.05.005, 2017.
- 405 Apel, E. C., Riemer, D. D., Hills, A., Baugh, W., Orlando, J., Faloona, I., Tan, D., Brune, W., Lamb,
406 B., Westberg, H., Carroll, M. A., Thornberry, T., and Geron, C. D.: Measurement and interpretation of
407 isoprene fluxes and isoprene, methacrolein, and methyl vinyl ketone mixing ratios at the PROPHET
408 site during the 1998 Intensive, Journal of Geophysical Research: Atmospheres, 107, ACH 7-1-ACH 7-
409 15, 10.1029/2000JD000225, 2002.
- 410 Atkinson, R.: Kinetics of the gas-phase reactions of OH radicals with alkanes and cycloalkanes,
411 Atmospheric Chemistry and Physics, 3, 2233-2307, 10.5194/acp-3-2233-2003, 2003.
- 412 Atkinson, R., and Arey, J.: Atmospheric degradation of volatile organic compounds, Chemical Reviews,
413 103, 4605-4638, 10.1021/cr0206420, 2003.
- 414 Carlton, A. G., Wiedinmyer, C., and Kroll, J. H.: A review of Secondary Organic Aerosol (SOA)
415 formation from isoprene, Atmospheric Chemistry and Physics, 9, 4987-5005, DOI 10.5194/acp-9-4987-
416 2009, 2009.
- 417 Chan, A. W. H., Kautzman, K. E., Chhabra, P. S., Surratt, J. D., Chan, M. N., Crounse, J. D., Kuerten,
418 A., Wennberg, P. O., Flagan, R. C., and Seinfeld, J. H.: Secondary organic aerosol formation from
419 photooxidation of naphthalene and alkynaphthalenes: implications for oxidation of intermediate
420 volatility organic compounds (IVOCs), Atmospheric Chemistry and Physics, 9, 3049-3060,
421 10.5194/acp-9-3049-2009, 2009.
- 422 Chan, A. W. H., Isaacman, G., Wilson, K. R., Worton, D. R., Ruehl, C. R., Nah, T., Gentner, D. R.,
423 Dallmann, T. R., Kirchstetter, T. W., Harley, R. A., Gilman, J. B., Kuster, W. C., deGouw, J. A.,
424 Offenberg, J. H., Kleindienst, T. E., Lin, Y. H., Rubitschun, C. L., Surratt, J. D., Hayes, P. L., Jimenez,
425 J. L., and Goldstein, A. H.: Detailed chemical characterization of unresolved complex mixtures in
426 atmospheric organics: Insights into emission sources, atmospheric processing, and secondary organic

427 aerosol formation, Journal of Geophysical Research-Atmospheres, 118, 6783-6796,
428 10.1002/jgrd.50533, 2013.

429 de Gouw, J. A., Gilman, J. B., Kim, S. W., Lerner, B. M., Isaacman-VanWertz, G., McDonald, B. C.,
430 Warneke, C., Kuster, W. C., Lefer, B. L., Griffith, S. M., Dusant, S., Stevens, P. S., and Stutz, J.:
431 Chemistry of Volatile Organic Compounds in the Los Angeles basin: Nighttime Removal of Alkenes
432 and Determination of Emission Ratios, Journal of Geophysical Research-Atmospheres, 122, 11843-
433 11861, 10.1002/2017jd027459, 2017.

434 Edney, E. O., Kleindienst, T. E., Jaoui, M., Lewandowski, M., Offenberg, J. H., Wang, W., and Claeys,
435 M.: Formation of 2-methyl tetrols and 2-methylglyceric acid in secondary organic aerosol from
436 laboratory irradiated isoprene/NO_x/SO₂/air mixtures and their detection in ambient PM2.5 samples
437 collected in the eastern United States, Atmospheric Environment, 39, 5281-5289,
438 <https://doi.org/10.1016/j.atmosenv.2005.05.031>, 2005.

439 Gentner, D. R., Isaacman, G., Worton, D. R., Chan, A. W. H., Dallmann, T. R., Davis, L., Liu, S., Day,
440 D. A., Russell, L. M., Wilson, K. R., Weber, R., Guha, A., Harley, R. A., and Goldstein, A. H.:
441 Elucidating secondary organic aerosol from diesel and gasoline vehicles through detailed
442 characterization of organic carbon emissions, Proceedings of the National Academy of Sciences of the
443 United States of America, 109, 18318-18323, 10.1073/pnas.1212272109, 2012.

444 Hayes, P. L., Ortega, A. M., Cubison, M. J., Froyd, K. D., Zhao, Y., Cliff, S. S., Hu, W. W., Toohey,
445 D. W., Flynn, J. H., Lefer, B. L., Grossberg, N., Alvarez, S., Rappenglueck, B., Taylor, J. W., Allan, J.
446 D., Holloway, J. S., Gilman, J. B., Kuster, W. C., De Gouw, J. A., Massoli, P., Zhang, X., Liu, J., Weber,
447 R. J., Corrigan, A. L., Russell, L. M., Isaacman, G., Worton, D. R., Kreisberg, N. M., Goldstein, A. H.,
448 Thalman, R., Waxman, E. M., Volkamer, R., Lin, Y. H., Surratt, J. D., Kleindienst, T. E., Offenberg, J.
449 H., Dusant, S., Griffith, S., Stevens, P. S., Brioude, J., Angevine, W. M., and Jimenez, J. L.: Organic
450 aerosol composition and sources in Pasadena, California, during the 2010 CalNex campaign, Journal of
451 Geophysical Research-Atmospheres, 118, 9233-9257, 10.1002/jgrd.50530, 2013.

452 Kleindienst, T. E., Edney, E. O., Lewandowski, M., Offenberg, J. H., and Jaoui, M.: Secondary Organic
453 Carbon and Aerosol Yields from the Irradiations of Isoprene and α -Pinene in the Presence of NO_x and
454 SO₂, Environmental Science & Technology, 40, 3807-3812, 10.1021/es052446r, 2006.

- 455 Lamkaddam, H., Gratien, A., Pangui, E., Cazaunau, M., Picquet-Varrault, B., and Doussin, J.-F.: High-
456 NOx Photooxidation of n-Dodecane: Temperature Dependence of SOA Formation, Environmental
457 Science & Technology, 51, 192-201, 10.1021/acs.est.6b03821, 2017a.
- 458 Lamkaddam, H., Gratien, A., Pangui, E., Cazaunau, M., Picquet-Varrault, B., and Doussin, J. F.: High-
459 NOx Photooxidation of n-Dodecane: Temperature Dependence of SOA Formation, Environ Sci
460 Technol, 51, 192-201, 10.1021/acs.est.6b03821, 2017b.
- 461 Li, L., Tang, P., Nakao, S., Kacarab, M., and Cocker, D. R., III: Novel Approach for Evaluating
462 Secondary Organic Aerosol from Aromatic Hydrocarbons: Unified Method for Predicting Aerosol
463 Composition and Formation, Environmental Science & Technology, 50, 6249-6256,
464 10.1021/acs.est.5b05778, 2016.
- 465 Lim, Y. B., and Ziemann, P. J.: Effects of Molecular Structure on Aerosol Yields from OH Radical-
466 Initiated Reactions of Linear, Branched, and Cyclic Alkanes in the Presence of NOx, Environmental
467 Science & Technology, 43, 2328-2334, 10.1021/es803389s, 2009.
- 468 Loza, C. L., Craven, J. S., Yee, L. D., Coggon, M. M., Schwantes, R. H., Shiraiwa, M., Zhang, X.,
469 Schilling, K. A., Ng, N. L., Canagaratna, M. R., Ziemann, P. J., Flagan, R. C., and Seinfeld, J. H.:
470 Secondary organic aerosol yields of 12-carbon alkanes, Atmospheric Chemistry and Physics, 14, 1423-
471 1439, 10.5194/acp-14-1423-2014, 2014.
- 472 Ng, N. L., Kroll, J. H., Chan, A. W. H., Chhabra, P. S., Flagan, R. C., and Seinfeld, J. H.: Secondary
473 organic aerosol formation from m-xylene, toluene, and benzene, Atmospheric Chemistry and Physics,
474 7, 3909-3922, DOI 10.5194/acp-7-3909-2007, 2007.
- 475 Pandis, S. N., Paulson, S. E., Seinfeld, J. H., and Flagan, R. C.: Aerosol formation in the photooxidation
476 of isoprene and β -pinene, Atmospheric Environment. Part A. General Topics, 25, 997-1008,
477 [https://doi.org/10.1016/0960-1686\(91\)90141-S](https://doi.org/10.1016/0960-1686(91)90141-S), 1991.
- 478 Presto, A. A., Miracolo, M. A., Donahue, N. M., and Robinson, A. L.: Secondary organic aerosol
479 formation from high-NO(x) photo-oxidation of low volatility precursors: n-alkanes, Environ Sci
480 Technol, 44, 2029-2034, 10.1021/es903712r, 2010a.

481 Presto, A. A., Miracolo, M. A., Donahue, N. M., and Robinson, A. L.: Secondary Organic Aerosol
482 Formation from High-NO_x Photo-Oxidation of Low Volatility Precursors: n-Alkanes, Environmental
483 Science & Technology, 44, 2029-2034, 10.1021/es903712r, 2010b.

484 Roberts, J., Marchewka, M., Bertman, S., Goldan, P., Kuster, W., de Gouw, J., warneke, C., Williams,
485 E., Lerner, B., Murphy, P., Apel, E., and Fehsenfeld, F.: Analysis of the isoprene chemistry observed
486 during the New England Air Quality Study (NEAQS) 2002 Intensive Experiment, Journal of
487 Geophysical Research-Atmospheres, 111, D23S12, 10.1029/2006JD007570, 2006.

488 Tajuelo, M., Rodriguez, D., Teresa Baeza-Romero, M., Diaz-de-Mera, Y., Aranda, A., and Rodriguez,
489 A.: Secondary organic aerosol formation from styrene photolysis and photooxidation with hydroxyl
490 radicals, Chemosphere, 231, 276-286, 10.1016/j.chemosphere.2019.05.136, 2019.

491 Tkacik, D. S., Presto, A. A., Donahue, N. M., and Robinson, A. L.: Secondary Organic Aerosol
492 Formation from Intermediate-Volatility Organic Compounds: Cyclic, Linear, and Branched Alkanes,
493 Environmental Science & Technology, 46, 8773-8781, 10.1021/es301112c, 2012.

494 Wolfe, G. M., Marvin, M. R., Roberts, S. J., Travis, K. R., and Liao, J.: The Framework for 0-D
495 Atmospheric Modeling (F0AM) v3.1, Geoscientific Model Development, 9, 3309-3319, 10.5194/gmd-
496 9-3309-2016, 2016.

497 Worton, D. R., G. Isaacman, D. R. Gentner, T. R. Dallmann, A. W. H. Chan, C. Ruehl, T. W.
498 Kirchstetter, K. R. Wilson, R. A. Harley and A. H. Goldstein: Lubricating Oil Dominates Primary
499 Organic Aerosol Emissions from Motor Vehicles. Environmental Science & Technology, 48(7): 3698-
500 3706, 10.1021/es405375j, 2014.

501 Zhang, X., Cappa, C. D., Jathar, S. H., McVay, R. C., Ensberg, J. J., Kleeman, M. J., and Seinfeld, J.
502 H.: Influence of vapor wall loss in laboratory chambers on yields of secondary organic aerosol,
503 Proceedings of the National Academy of Sciences of the United States of America, 111, 5802-5807,
504 10.1073/pnas.1404727111, 2014.

505